

# Storms and the Depletion of Ammonia in Jupiter: I. Microphysics of “Mushballs”

Tristan Guillot<sup>1,2</sup>, David J. Stevenson<sup>3</sup>, Sushil K. Atreya<sup>4</sup>, Scott J. Bolton<sup>5</sup>,  
Heidi N. Becker<sup>6</sup>

<sup>1</sup>Université Côte d’Azur, OCA, Lagrange CNRS, 06304 Nice, France

<sup>2</sup>The University of Tokyo, Department of Earth and Planetary Science, Tokyo 113-0033, Japan

<sup>3</sup>California Institute of Technology, Pasadena, CA 91125, USA

<sup>4</sup>University of Michigan, Ann Arbor, MI 48109, USA

<sup>5</sup>Southwest Research Institute, San Antonio, Texas, USA

<sup>6</sup>Jet Propulsion Laboratory, California Institute of Technology, Pasadena, CA 91109, USA

## Key Points:

- We show that ammonia can melt water-ice crystals in Jupiter’s powerful storms and lead to the formation of water-ammonia hailstones (mushballs)
- These mushballs and subsequent downdrafts transport ammonia to very deep levels
- This can potentially explain Juno measurements that Jupiter’s ammonia abundance is variable until at least 150km below the visible clouds.

This is the author manuscript accepted for publication and has undergone full peer review but has not been through the copyediting, typesetting, pagination and proofreading process, which may lead to differences between this version and the [Version of Record](#). Please cite this article as doi: [10.1029/2020JE006403](https://doi.org/10.1029/2020JE006403)

Corresponding author: Tristan Guillot, [tristan.guillot@oca.eu](mailto:tristan.guillot@oca.eu)

**Abstract**

Microwave observations by the Juno spacecraft have shown that, contrary to expectations, the concentration of ammonia is still variable down to pressures of tens of bars in Jupiter. We show that during strong storms able to loft water ice into a region located at pressures between 1.1 and 1.5 bar and temperatures between 173K and 188K, ammonia vapor can dissolve into water ice to form a low-temperature liquid phase containing about 1/3 ammonia and 2/3 water. We estimate that, following the process creating hailstorms on Earth, this liquid phase enhances the growth of hail-like particles that we call mushballs. We develop a simple model to estimate the growth of these mushballs, their fall into Jupiter's deep atmosphere and their evaporation. We show that they evaporate deeper than the expected water cloud base level, between 5 and 27 bar depending on the assumed abundance of water ice lofted by thunderstorms and on the assumed ventilation coefficient governing heat transport between the atmosphere and the mushball. Because the ammonia is located mostly in the core of the mushballs, it tends to be delivered deeper than water, increasing the efficiency of the process. Further sinking of the condensates is expected due to cold temperature and ammonia- and water-rich downdrafts formed by the evaporation of mushballs. This process can thus potentially account for the measurements of ammonia depletion in Jupiter's deep atmosphere.

**Plain Language Summary**

The Juno mission has revealed that Jupiter's atmosphere is much more complex and intriguing than previously anticipated. Most of Jupiter's atmosphere was shown to be depleted in ammonia. While ammonia was expected to be well mixed, large scale variability of ammonia was detected at least 100 km below the cloud level where condensation occurs. We propose a mechanism to explain this depletion and variability. We show that in Jupiter, at very low temperatures (of order  $-90^{\circ}\text{C}$ ), water ice and ammonia vapor combine to form a liquid and we hypothesize that this subsequently triggers unexpected meteorology. During Jupiter's violent storms, hailstones form from this liquid, similar to the process in terrestrial storms where hail forms in the presence of supercooled liquid water. Growth of the hailstones creates a slush-like substance surrounded by a layer of ice, and these "mushballs" fall, evaporate, and continue sinking further in the planet's deep atmosphere, creating both ammonia depletion and variability, potentially explaining the Juno observations.

**1 Introduction**

Ammonia condenses in Jupiter's atmosphere at pressures lower than about 0.8 bar and would be expected to be uniformly mixed below that level (Atreya et al., 1999). Ground-based VLA radio-wave observations have shown that, in several regions of the atmosphere, ammonia is depleted down to at least several bars (de Pater et al., 2016, 2019). MWR (Microwave Radiometer) observations from Juno (Bolton et al., 2017; Li et al., 2017) show that the depletion extends throughout the mid latitudes, is variable and is much more prevalent than previously reported, reaching very deep levels: At mid-latitudes, the volume mixing ratio of ammonia remains relatively low (between about 120 to 250 ppmv) until it increases to a value  $\sim 360$  ppmv at pressures greater than 20-30 bars. In the northern component of Jupiter's Equatorial Zone, at latitudes between 0 and  $5^{\circ}\text{N}$ , the mixing ratio is relatively uniform vertically and equal to  $\sim 360$  ppmv. Such a global change in ammonia abundance cannot be explained solely by meridional circulation because it would violate mass balance (Ingersoll et al., 2017). A local depletion of ammonia down to 4-6 bars may be explained by updrafts and compensating subsidence (Showman & de Pater, 2005), but this process cannot

67 extend much deeper below the water cloud base and is thus unable to account for the  
68 Juno measurements.

69 We propose a scenario that can account for the observed vertical and latitudinal  
70 dependence of the ammonia concentration. In this paper, we show that during strong  
71 storms, ammonia in Jupiter can dissolve into water-ice crystals at temperatures around  
72  $-90^{\circ}\text{C}$ , subsequently leading to the formation of partially melted hailstones that we  
73 call 'mushballs', and to their transport to great depths. In a second paper, we will  
74 apply this scenario to explain the Juno MWR measurements.

75 In Section 2 we first investigate the interaction between ammonia vapor and  
76 water-ice crystals. We then calculate in Section 3 the growth and transport of the  
77 'mushballs' thus formed. We discuss in Section 4 how further downward transport  
78 of ammonia- and water-rich gas must result from evaporative cooling and subsequent  
79 downdrafts.

## 80 2 The interaction between ammonia vapor and water-ice crystals

### 81 2.1 The $\text{NH}_3\text{-H}_2\text{O}$ phase diagram

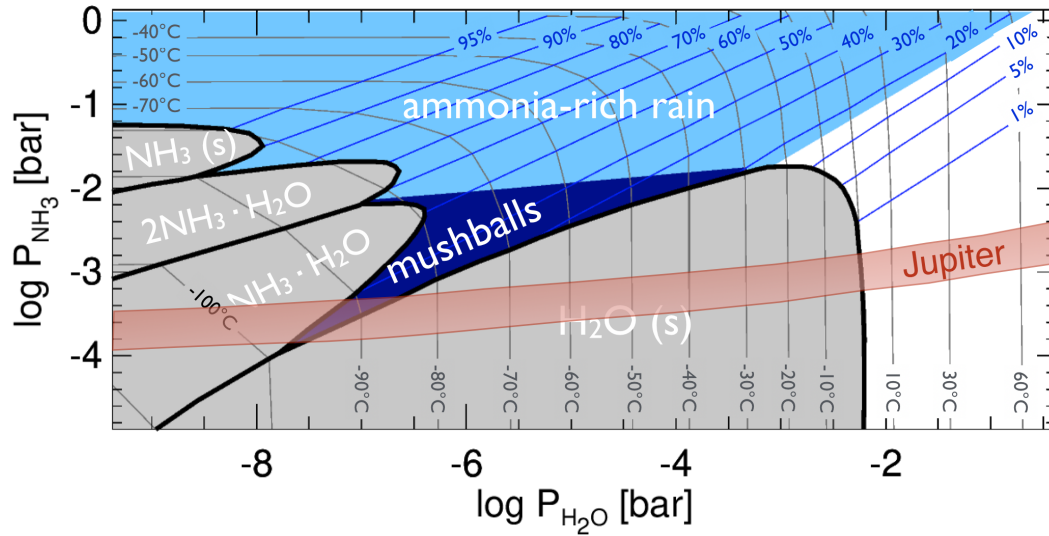
82 Ammonia is known to dissolve easily into liquid water, a consequence of similar  
83 dielectric properties of the two molecules. This has been recognized early on (Lewis,  
84 1969; Weidenschilling & Lewis, 1973) and led to the current models of Jupiter's cloud  
85 structure which state that at pressures levels between 2 and 9 bars, depending on the  
86  $\text{H}_2\text{O}$  abundance, a water-cloud layer is formed, and some ammonia is dissolved into  
87 liquid water droplets forming a weak aqueous ammonia solution cloud (Atreya et al.,  
88 1999). The amount dissolved is however small: At  $-20^{\circ}\text{C}$  (corresponding to a  $\sim 4$  bar  
89 pressure level in Jupiter) equilibrium chemistry predicts that a maximum of only 3%  
90 of ammonia can dissolve into supercooled liquid water droplets (Ingersoll et al., 2017).  
91 Deeper in the atmosphere, at higher temperatures, ammonia solubility decreases while  
92 at higher elevations water freezes and should not include any significant amount of  
93 ammonia. Given the solar O/N ratio of 7.2 (Lodders, 2003) it is difficult to imagine  
94 how rainstorms could affect in any significant way the ammonia budget (Ingersoll et  
95 al., 2017).

96 However, in the same pioneering article about Jupiter clouds, John S. Lewis  
97 states:

98 *"It is not as commonly known that the freezing point of aqueous  $\text{NH}_3$  can be depressed*  
99 *as low as  $-100.3^{\circ}\text{C}$ , and that the solid phases formed upon freezing of concentrated  $\text{NH}_3$*   
100 *solution can be  $\text{NH}_3\cdot\text{H}_2\text{O}$  or  $2\text{NH}_3\cdot\text{H}_2\text{O}$ , not necessarily solid  $\text{NH}_3$  or  $\text{H}_2\text{O}$ ".*

101 In Fig. 1, we reproduce the  $\text{NH}_3\text{-H}_2\text{O}$  phase diagram of Weidenschilling and  
102 Lewis (1973), showing solid phases in grey (from left to right,  $\text{NH}_3$  ice,  $2\text{NH}_3\cdot\text{H}_2\text{O}$  ice,  
103  $\text{NH}_3\cdot\text{H}_2\text{O}$  ice and  $\text{H}_2\text{O}$  ice) and liquid  $\text{NH}_3\cdot\text{H}_2\text{O}$  in white and blue colors. (The solid  
104  $\text{NH}_3\cdot 2\text{H}_2\text{O}$  phase discovered later –see Kargel (1992) – is not included, but will not  
105 affect the results of the present work). The concentration of ammonia in the aqueous  
106 solution decreases from left to right from over 95% in the upper left to less than 1%  
107 in the lower right. Using the pressure temperature profile  $P(T)$  measured in Jupiter by  
108 the Galileo probe (Seiff et al., 1998) and a given volume mixing ratio  $x_{\text{NH}_3}$  of ammonia,  
109 we can readily calculate the partial pressure of ammonia as a function of temperature  
110 in Jupiter, i.e.  $P_{\text{NH}_3}(T) = x_{\text{NH}_3}P(T)$ . The result for  $x_{\text{NH}_3}$  between 100 and 360 ppmv,  
111 the approximate range of ammonia mixing ratios measured by Juno (Li et al., 2017)  
112 is shown as a red ribbon in Fig. 1.

113 Let us follow the upward motion of a water droplet formed below the 5-bar level  
114 in Jupiter's deep atmosphere by following the red ribbon in Fig. 1 from right to left. As  
115 liquid, it can dissolve a small fraction of ammonia - but this fraction remains smaller



**Figure 1.**  $\text{H}_2\text{O}$ - $\text{NH}_3$  equilibrium phase diagram (Weidenschilling & Lewis, 1973) as a function of partial pressure of  $\text{H}_2\text{O}$  and  $\text{NH}_3$ . Solid phases are indicated in grey, otherwise, a liquid mixture forms with a concentration in ammonia indicated by the blue diagonal contour. The temperatures in Celsius are indicated as contour lines running from the bottom to the left of the plot. The red region labeled Jupiter corresponds to Jupiters atmosphere assuming a minimum  $\text{NH}_3$  abundance of 100 ppmv and a maximum value of 360 ppmv (Li et al., 2017).

116 than a percent in equilibrium conditions and reaches a few percent only by invoking  
 117 large supercooling of the water droplets to  $-20^\circ\text{C}$  or so, as obtained by Ingersoll  
 118 et al. (2017). When the droplet freezes to become an ice crystal, the equilibrium  
 119 solution predicts the existence of pure water ice, implying that any ammonia must  
 120 be expelled. However, when moving still higher up, in a region between 173 K and  
 121 188 K (i.e.,  $-100^\circ\text{C}$  to  $-85^\circ\text{C}$ ), equilibrium chemistry predicts that a liquid  $\text{H}_2\text{O}\cdot\text{NH}_3$   
 122 mixture with a 30% – 40% concentration of ammonia should form. Although this was  
 123 recognized early on, this possibility was never really considered for Jupiter because  
 124 of the fast rainout of water droplets and ice crystals (Lewis, 1969; Weidenschilling &  
 125 Lewis, 1973; Atreya et al., 1999). However models of water thunderstorms including  
 126 detailed microphysics show that storms are able to loft 100 ppmv of water ice to the 1  
 127 bar level in the form of 10– to 100 –  $\mu\text{m}$  particles (Yair et al., 1995). Storms so large  
 128 that they can reach the stratosphere have been observed and modelled as extended  
 129 water storms (Hueso et al., 2002; Sugiyama et al., 2014). These storms can last for  
 130 up to about ten days. They are believed to carry most of the intrinsic heat flux of the  
 131 planet (Gierasch et al., 2000).

132 Thus, although on average the abundance of water near the 1-bar level in Jupiter’s  
 133 atmosphere is extremely small, during large storms, conditions are met for the pres-  
 134 ence of a significant amount of ice in a region in which liquid  $\text{NH}_3\cdot\text{H}_2\text{O}$  may form. On  
 135 Earth, hail grows most rapidly in the presence of supercooled liquid water (Pruppacher  
 136 & Klett, 1997) - it is thus possible that on Jupiter large storms lead to the formation of  
 137 large  $\text{NH}_3\cdot\text{H}_2\text{O}$  condensates and their fall to deeper levels. Because the concentration  
 138 in ammonia can be large, up to 40%, this is a mechanism that can potentially deplete  
 139 ammonia from the upper atmosphere more efficiently than it depletes water. Interest-  
 140 ingly, at even higher levels (pressures lower than 1.2 bars), the equilibrium phase is a  
 141 solid  $\text{NH}_3\cdot\text{H}_2\text{O}$  condensate with an even higher ammonia concentration (up to 50%).

We name these condensates “mushballs” because we expect the presence of both solid and liquid phases containing variable amounts of ammonia and water and because the liquid phase thus formed is a highly viscous ‘mush’ (Kargel et al., 1991). Now let us examine whether they have time to form and grow.

## 2.2 Adsorption of ammonia into water-ice particles

Large thunderstorms on Jupiter can loft small-size ( $\sim 10 - 100 \mu\text{m}$ ) ice particles up to regions near a pressure of 1 bar (Yair et al., 1995). These storms develop over timescales of hours to days (Hueso et al., 2002). Can ammonia be efficiently adsorbed into these water-ice particles on these timescales?

Let us consider an icy  $\text{H}_2\text{O}$  particle that reached a level where equilibrium chemistry (Fig. 1) predicts the formation of a  $\text{NH}_3\text{-H}_2\text{O}$  liquid solution (e.g.,  $\sim 1.5$  bar,  $T \sim -85^\circ\text{C}$  for a vapor concentration of  $\text{NH}_3$   $x_{\text{NH}_3} \sim 300$  ppmv). An estimate of the timescale to melt the particle is obtained by dividing the number of  $\text{H}_2\text{O}$  molecules in the particle to the  $\text{NH}_3$  vapor collision rate. Because the mean free path of ammonia vapor  $\lambda_{\text{NH}_3} \sim 3D_{\text{NH}_3}/v_{\text{th}} \sim 0.1 \mu\text{m}$  ( $D_{\text{NH}_3} \sim 0.3 \text{cm}^2/\text{s}$  is the diffusion coefficient of ammonia in hydrogen and  $v_{\text{th}} \sim 1.2 \times 10^5 \text{cm/s}$  is the average gas velocity for this pressure level in Jupiter — see Table B1 in Appendix B) is much smaller than the size of the particles that we consider ( $10 - 100 \mu\text{m}$ ), the process is limited by diffusion effects. Given the small terminal velocity of the ice crystals (see Fig. 2 hereafter), they can be considered as co-moving with the gas. In this case, the timescale for the melting of an ice crystal by adsorption of ammonia vapor is (Davidovits et al., 2006)

$$\tau_{\text{ads}} = \frac{1}{36} r_{\text{NH}_3\text{-H}_2\text{O}} a_{\text{Kn}} \frac{\tilde{\rho}_{\text{H}_2\text{O}}}{\mu_{\text{H}_2\text{O}}} \sqrt{\frac{\mu_{\text{NH}_3}}{\mu}} \frac{\mathcal{R}T}{x_{\text{NH}_3} P} \frac{\tilde{d}^2}{D_{\text{NH}_3}} \approx 6 \left( \frac{\tilde{d}}{100 \mu\text{m}} \right)^2 \text{ s}, \quad (1)$$

where  $r_{\text{NH}_3\text{-H}_2\text{O}} \sim 1/2$  is the ratio of  $\text{NH}_3$  to  $\text{H}_2\text{O}$  molecules of the equilibrium mixture,  $a_{\text{Kn}} \sim 0.75$  results from an empirical fit (Davidovits et al., 2006),  $\tilde{\rho}_{\text{H}_2\text{O}}$  is the physical density of ice grains,  $\mu_{\text{H}_2\text{O}}$  and  $\mu_{\text{NH}_3}$  are the molar masses of  $\text{H}_2\text{O}$  and  $\text{NH}_3$  molecules respectively,  $\mu \sim 2.3 \text{g/mol}$  is the mean molar mass of the atmosphere,  $x_{\text{NH}_3} \sim 300$  ppmv is the molar abundance of  $\text{NH}_3$ ,  $P$  is pressure ( $\sim 1.5$  bar),  $T$  temperature ( $\sim 188 \text{K}$ ),  $\mathcal{R}$  the gas constant, and  $\tilde{d}$  is the ice grain diameter. Following measurements in Earth’s clouds (Pruppacher & Klett, 1997), we adopt  $\tilde{\rho}_{\text{H}_2\text{O}} \sim 0.3 \text{g/cm}^3$  but admittedly, this parameter is extremely uncertain.

While short, this timescale is longer by  $(a_{\text{Kn}}/2)(\tilde{d}/\lambda_{\text{NH}_3}) \sim 375(\tilde{d}/100 \mu\text{m})$  compared to a kinetic timescale (Davidovits et al., 2006). Experiments show that ammonia adsorption by ice crystal in vacuum is imperfect, i.e., the so-called uptake coefficient ranges between  $\alpha \sim 3 \times 10^{-4}$  to  $4 \times 10^{-3}$  at temperatures between 170 K and 190 K (Jin & Chu, 2007; Kasper et al., 2011). This could lead to a timescale one to two orders of magnitude higher than the above one. However, our situation is different because of melting. Based on liquid-droplet-train experiments (Davidovits et al., 2006), we expect in that case values of  $\alpha$  much closer to unity, implying that adsorption should be limited by diffusion.

Other limitations include the fact that only the partial pressure of  $\text{NH}_3$  above saturation contributes to the adsorption, and the fact that molecules at the surface must diffuse into the interior. The first effect is estimated from the distance to the pure  $\text{H}_2\text{O}$  ice curve in Fig. 1 to lead to a limited increase of timescale (decrease of partial vapor pressure) by a factor  $\sim 2$  across the mushball formation region. The latter is linked to the diffusion timescale inside the grain:  $\tau_{\text{diff}} \sim \tilde{d}^2/\tilde{D}_{\text{NH}_3}$ , where  $\tilde{D}_{\text{NH}_3}$  is the diffusion coefficient for  $\text{NH}_3$  inside the grain.

Let us consider diffusion of ammonia vapor through the liquid  $\text{NH}_3\text{-H}_2\text{O}$  surface layer. At room temperatures,  $\tilde{D}_{\text{NH}_3}^{\text{liq}} \sim 10^{-5} \text{cm}^2/\text{s}$ , but we must account that it is a

189 strong function of temperature. Laboratory measurements show that the viscosity of  
 190 the liquid  $\text{NH}_3\text{-H}_2\text{O}$  mixture increases by up to 3 orders of magnitude at  $T = 176.2\text{K}$   
 191 (Kargel et al., 1991) compared to room temperature. Owing to the Einstein relation,  
 192 we expect a comparable decrease of the diffusion coefficient, i.e., yielding  $\tilde{D}_{\text{NH}_3}^{\text{liq}} \sim$   
 193  $10^{-8}\text{ cm}^2/\text{s}$  in our case. This implies that small ice crystals of  $10\ \mu\text{m}$  sizes can be  
 194 melted in  $\sim 100$  seconds but that larger  $100\text{-}\mu\text{m}$  crystals could take up to several hours  
 195 to melt completely if they are compact. The melting time should be significantly  
 196 shorter if the water-ice crystals are porous.

197 We thus expect adsorption in the mushball-formation region to be limited by  
 198 diffusion effects so that  $\tau_{\text{ads}} \sim 100 \left( \tilde{d}/10\ \mu\text{m} \right)^2$  s. Assuming a  $50\text{ m/s}$  updraft,  $100\text{ s}$   
 199 corresponds to the expected crossing-time of the  $\sim 5\text{ km}$  mushball-formation region.  
 200 The lifetime of storms (at least hours) and the residence time of small particles (about  
 201  $1.5\text{ hr}$  for a  $100\ \mu\text{m}$  particle) indicate that ice crystals smaller than  $10$  to  $100\ \mu\text{m}$  should  
 202 be entirely melted by the adsorption of  $\text{NH}_3$  vapor.

203 We note that we did not consider the heat balance in the grain. Heat con-  
 204 duction takes place with a timescale  $\tau_{\text{cond}} \sim \tilde{d}^2 \tilde{\rho}_{\text{H}_2\text{O}} \tilde{c}_{P,\text{H}_2\text{O}} / \tilde{k}_{\text{H}_2\text{O}}$  where  $\tilde{c}_{P,\text{H}_2\text{O}} \sim$   
 205  $1.5 \times 10^7\text{ erg g}^{-1}\text{ K}^{-1}$  is the heat capacity of water ice at  $-80^\circ\text{C}$  and  $\tilde{k}_{\text{H}_2\text{O}} \sim 3.2 \times$   
 206  $10^5\text{ erg s}^{-1}\text{ K}^{-1}\text{ cm}^{-1}$  its thermal conductivity. Thus for the small grains considered  
 207 heat conduction takes place on a timescale  $\tau_{\text{cond}} \sim 10^{-3}\text{ s}$ , i.e., extremely fast com-  
 208 pared to the other timescales. We note however that this ignores latent heat effects  
 209 which should also be considered.

### 210 3 Growth and transport of mushballs

#### 211 3.1 Fall velocities

212 Let us first examine how particles may be lofted by updrafts or fall because of  
 213 a too large mass in Jupiter's atmosphere. The terminal velocity of particles falling in  
 214 the atmosphere is obtained from the equilibrium between drag force and gravitational  
 215 acceleration. It is conveniently expressed as:

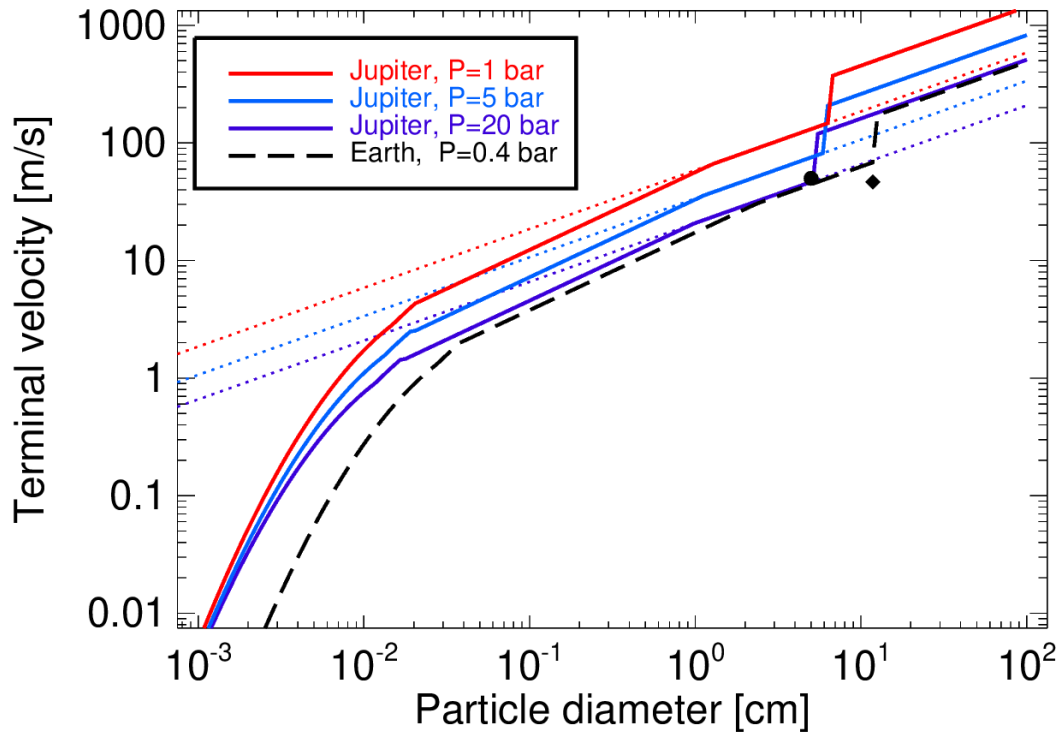
$$216 \quad v_{\text{fall}} = \left( \frac{4}{3C_d} \frac{\tilde{\rho}g\tilde{d}}{\rho_a} \right)^{1/2}, \quad (2)$$

217 where  $\tilde{d}$  is the particle size,  $\tilde{\rho}$  its physical density,  $g$  the gravitational acceleration,  $\rho_a$   
 218 the atmospheric density and  $C_d$  is the dimensionless drag coefficient. For hard spheres,  
 219  $\tilde{d}$  is the diameter and  $C_d$  is only a function of the Reynolds number of the particle,  
 220 defined as  $N_{\text{Re}} = \tilde{d}\rho_a v_{\text{fall}}/\eta_a$ , with  $\eta_a$  being the dynamic viscosity of the atmosphere.  
 221 For large spheres (mm-size or more in our case),  $C_d \sim 0.47$ , but in the general case this  
 222 is a function of  $N_{\text{Re}}$ , and of the shape of the particle (Pruppacher & Klett, 1997). We  
 223 use the formulation of  $C_d(N_{\text{Re}})$  of Rasmussen and Heymsfield (1987) based on studies  
 224 of hailstones on Earth. (We correct a typo (a forgotten minus sign) in Eq. (B1) of  
 Rasmussen and Heymsfield (1987):  $\log_{10} N_{\text{Re}} = -1.7095 + 1.33438W - 0.11591W^2$ .)

225 We will see that large hailstones/mushballs in Jupiter can reach large Reynolds  
 226 numbers. It is known experimentally that above a value  $N_{\text{Re,crit}} \approx 3 \times 10^5$ , the drag  
 227 coefficient suddenly drops by a factor  $\sim 5$ . While this is generally not the case on  
 228 Earth for hailstones (Rasmussen & Heymsfield, 1987; Roos, 1972), it is of relevance to  
 229 golf and tennis balls (Kundu & Cohen, 2016) and probably of mushballs in Jupiter.  
 230 We therefore include the effect by imposing that for  $N_{\text{Re}} > 3 \times 10^5$ ,  $C_d = 0.1$ . (As we  
 231 will see, this level of simplification is sufficient for our purposes).

232 Fig. 2 shows how the terminal velocity of particles (assumed dense and spherical)  
 233 varies with size at various levels in Jupiter atmosphere, and on Earth. Due to Jupiters  
 234 higher gravity and lower molecular weight of its atmosphere, terminal velocities are





**Figure 2.** Terminal velocity of ice (or ammonia-ice) particles with diameters from  $1 \mu\text{m}$  to  $1\text{m}$ , for three pressure levels, 1, 5 and 20 bar inside Jupiters atmosphere. The plain lines correspond to the full formulation. The dotted lines are the result from assuming a constant drag  $C_d=0.6$ , applicable to large Earth hailstones (Rasmussen & Heymsfield, 1987). For comparison the Earth case for a pressure of 400 mbar and a temperature of  $-20^\circ\text{C}$  is shown as a dashed line. Two examples for the Earth case are shown: The circle corresponds to 5cm hailstones observed in a particularly powerful storm which occurred in Oklahoma on 1976/05/29, with updrafts of  $\sim 50\text{m/s}$  (Nelson, 1983). The diamond corresponds to a giant hailstone collected on 1970/09/03 also in Oklahoma, weighting 766 g, with 15.5 cm of longest dimension and 11.8 cm of effective diameter (Roos, 1972).

about 4 times larger than on Earth for the same pressure level. For sizes below  $100 \mu\text{m}$ , we are in the Stokes regime, implying  $C_d \sim 24/N_{\text{Re}}$  and  $v_{\text{fall}} \propto \tilde{d}^2$ . The fall velocities are slower than 1 m/s. At larger sizes,  $C_d$  decreases to reach a value measured to be  $C_d \sim 0.6$  for real hailstones (Rasmussen & Heymsfield, 1987). At larger sizes, when reaching the critical Reynolds number  $N_{\text{Re,crit}}$ , the terminal velocity is expected to increase suddenly, which is represented by a kink in Fig. 2. A near-critical giant hailstone of 766 g was collected in Oklahoma and found to be slightly sub-critical (Roos, 1972), with a terminal velocity measured in wind tunnels reaching 44 to 47 m/s, slightly below our theoretical curve (this can be attributed to its complex shape). On Jupiter, because of a higher kinematic viscosity, the critical Reynolds number is reached for particle sizes about 3 times smaller than on Earth, i.e., for particle diameters above 4 to 6 cm.

We may distinguish three types of condensed particles:

- Cloud droplets and ice crystals: On Earth, most have sizes between 10 and  $50 \mu\text{m}$  (Pruppacher & Klett, 1997; Rogers & Yau, 1996). Similar values are found in models of Jupiter water clouds using realistic microphysics, but with a tendency for a faster growth and thus slightly larger sizes  $\sim 100 \mu\text{m}$  or more (Yair et al., 1995).
- Raindrops: Their maximum diameter is set by hydrodynamical stability considerations:  $\tilde{d} \sim (\gamma/\tilde{\rho}g)^{1/2}$ , where  $\gamma$  is surface tension,  $\tilde{\rho}$  is density of the liquid. We expect surface tension to be only weakly affected by ammonia content and temperature, implying that since on Earth the maximum droplet diameter is about 5 mm, it should be of order 3 mm on Jupiter due to its larger gravity. These maximum droplet sizes should fall with a velocity  $\sim 20 \text{ m/s}$  at 5 bar.
- Hailstones/mushballs: They can reach large sizes, provided that the updraft velocity balances their terminal velocity. Of course, this also requires fast growth, something that is obtained on Earth when supercooled water is present to allow an efficient sticking of droplets. The circle in Fig. 2 corresponds to the maximum hailstone diameter in a powerful hailstorm which occurred in Oklahoma in 1976 and for which the maximum updraft speed was measured to be  $50 \text{ m/s}$  (Nelson, 1983). This value corresponds to the terminal velocity of these largest hailstones, showing that balance between updraft speed and terminal velocity is key. Given storms with updraft speed ranging from 10 to  $100 \text{ m/s}$  in Jupiter (Stoker, 1986; Hueso et al., 2002; Sugiyama et al., 2014), we should expect hailstones in Jupiter to be able, in principle, to reach similar sizes as on Earth.

### 3.2 Growth of mushballs

We now examine how initially small ( $\sim 100 \mu\text{m}$ ) water-ice crystals in a strong ( $\sim 50 \text{ m/s}$ ) updraft may adsorb ammonia, grow, collect more icy particles until they become too large to remain part of the updraft and begin to fall. Although this model is simple and may be considered naive in regard to the complexity of hail formation on Earth (Pruppacher & Klett, 1997), we believe that the framework presented here provides a useful insight into the Earth-like phenomena taking place in Jupiter's atmosphere and should help to explain Juno's observations.

The adsorption of  $\text{NH}_3$  vapor by ice particles is expected to be heterogeneous, a consequence of the temperature gradients between the core of the updraft which should be warmer by up to  $\sim 5 \text{ K}$  compared to the outside. The ammonia adsorption and resulting melting of the ice particles should occur faster towards the edge of updrafts because of the entrainment of this colder surrounding atmosphere.

Prior to reaching the 1.5-bar level, the growth of ice particles in the updraft could be considered as essentially stalled: larger particles having rained out, only small-size



particles (between 1 and 100  $\mu\text{m}$ ) remain and have a low collision probability (Yair et al., 1995). Crossing the mushball-formation region suddenly has two effects: The adsorption of ammonia vapor increases particle mass by 30%. Melting also increases their density from low values (say  $\sim 0.3 \text{ g/cm}^3$ ) (Davidovits et al., 2006) to that of the liquid ammonia-water mixture, i.e.  $0.9 \text{ g/cm}^3$ . Both processes lead to an increase of the fall velocity for these particles. For example, at the 1.5-bar level, the terminal velocity of a 30- $\mu\text{m}$  ice particle with a density of  $0.3 \text{ g/cm}^3$  is about 2.5 m/s, it grows to 2.7 m/s due to mass increase and to 3.9 m/s due to melting, an overall 60% increase. It is natural to assume that because of cloud heterogeneity, the differential velocities of the particles will quickly increase.

In what follows we will use a simplified approach, by considering that, in an updraft of velocity  $v_{\text{up}}$ , one particle (hereafter “mushball”) of mass  $\tilde{m}$ , diameter  $\tilde{d}$  and terminal velocity  $v_{\text{fall}}$  grows at the expense of other particles (hereafter “cloud droplets”) with comparatively much smaller terminal velocities. The mass of the mushball, its altitude  $z$  and ammonia mixing ratio evolve with time according to the following relations:

$$\frac{d\tilde{M}_{\text{H}_2\text{O}}}{dt} = E \frac{\pi}{4} \tilde{d}^2 \mu_{\text{H}_2\text{O}} \tilde{x}_{\text{H}_2\text{O}} \frac{P}{\mathcal{R}T} v_{\text{fall}}, \quad (3)$$

$$\frac{d\tilde{M}_{\text{NH}_3}}{dt} = E \frac{\pi}{4} \tilde{d}^2 \mu_{\text{NH}_3} \tilde{x}_{\text{NH}_3} \frac{P}{\mathcal{R}T} v_{\text{fall}}, \quad (4)$$

$$\frac{dz}{dt} = v_{\text{up}} - v_{\text{fall}}, \quad (5)$$

where  $\tilde{M}_{\text{H}_2\text{O}}$  and  $\tilde{M}_{\text{NH}_3}$  are the mushball masses in water and ammonia, respectively,  $\mu_{\text{H}_2\text{O}}$  and  $\mu_{\text{NH}_3}$  the molecular masses,  $\tilde{x}_{\text{H}_2\text{O}}$  and  $\tilde{x}_{\text{NH}_3}$  their volume mixing ratios in the condensed phase (as cloud droplets), and  $E$  is the collection efficiency. Since we assume sphericity mass and diameter are related by  $\tilde{M} = \tilde{M}_{\text{H}_2\text{O}} + \tilde{M}_{\text{NH}_3} = (\pi/6)\tilde{\rho}\tilde{d}^3$  where  $\tilde{\rho}$  is the physical density of the mushball.

The value of  $\tilde{x}_{\text{H}_2\text{O}}$ , the mixing ratio of condensed water, is set by the ability of the storm to loft small icy particles to the region considered. Because at the temperatures that we consider, the vapor pressure of water is extremely low (see fig. 1), we assume that  $\tilde{x}_{\text{H}_2\text{O}} = x_{\text{H}_2\text{O}}$ , the total mixing ratio of water. Yair et al. (1995) find a mass mixing ratio of water at the 1 bar level that can reach 1 g/kg, corresponding to  $\tilde{x}_{\text{H}_2\text{O}} = 133$  ppmv. This value is obtained for a solar-composition atmosphere and should increase for a higher deep abundance of water. We also note that higher values are likely due to a feedback mechanism not considered in that study: The formation of mushballs can increase updraft speed by decreasing condensate load at depth and by creating strong horizontal temperature gradients upon melting and evaporation. On the other hand, cloud-ensemble simulations (Sugiyama et al., 2014) using the so-called Kessler parameterization of microphysical processes (Kessler, 1969) impose a conversion rate from non-precipitating condensates to precipitating condensates that cannot be used to reliably predict the amount of small-size particles at high altitudes. We thus adopt three possible values of  $\tilde{x}_{\text{H}_2\text{O}}$ , 100, 600 and 1200 ppmv.

The value of  $\tilde{x}_{\text{NH}_3}$ , the mixing ratio of condensed ammonia, is set by the abundance of ammonia vapor  $x_{\text{NH}_3}$ , the value of  $\tilde{x}_{\text{H}_2\text{O}}$  and the location in the phase diagram set by the pressure and temperature conditions. We consider that  $\tilde{x}_{\text{NH}_3} = 0$  in the pure  $\text{H}_2\text{O}$  ice region of the phase diagram. Mushballs start forming when liquid  $\text{H}_2\text{O}\cdot\text{NH}_3$  forms, at pressures  $P \lesssim 1.5$  bar and temperatures  $T \lesssim 188$  K for  $x_{\text{NH}_3} = 360$  ppmv, corresponding to the global ammonia abundance of the north Equatorial Zone (Li et al., 2017). In order to calculate  $\tilde{x}_{\text{NH}_3}$ , we determine for the temperature of the levels considered the intersections with the pure  $\text{H}_2\text{O}$  ice phase and with the  $\text{H}_2\text{O}\cdot\text{NH}_3$  ice phase. We derive the corresponding values of the ammonia vapor mixing ratio,  $x_1$  and  $x_2$ , respectively. If  $x_1 < x_{\text{NH}_3} \leq x_2$  the equilibrium is between  $\text{H}_2\text{O}\cdot\text{NH}_3$  liquid

331 and H<sub>2</sub>O ice. If  $x_2 < x_{\text{NH}_3}$ , at temperatures  $T \lesssim 170\text{K}$ , it is between H<sub>2</sub>O·NH<sub>3</sub> ice,  
 332 H<sub>2</sub>O·NH<sub>3</sub> liquid and H<sub>2</sub>O ice. By assuming full thermodynamic equilibrium and that  
 333 H<sub>2</sub>O·NH<sub>3</sub> liquid contains 2/3 H<sub>2</sub>O and 1/3 NH<sub>3</sub>, we derive

$$\tilde{x}_{\text{NH}_3} = \begin{cases} 0 & \text{if } x_{\text{NH}_3} \leq x_1, \\ \min [x_{\text{NH}_3} - x_1, \tilde{x}_{\text{H}_2\text{O}}/2] & \text{if } x_1 < x_{\text{NH}_3} \leq x_2, \\ \min [x_{\text{NH}_3} - x_1, \tilde{x}_{\text{H}_2\text{O}} + (x_{\text{NH}_3} - x_2)/2, \tilde{x}_{\text{H}_2\text{O}}] & \text{if } x_{\text{NH}_3} > x_2. \end{cases} \quad (6)$$

334 Based on the values of  $\tilde{M}_{\text{H}_2\text{O}}$  and  $\tilde{M}_{\text{NH}_3}$ , we can calculate the mass fraction of  
 335 ammonia in the mushballs

$$\tilde{f}_{\text{NH}_3} = \frac{\tilde{M}_{\text{NH}_3}}{\tilde{M}_{\text{NH}_3} + \tilde{M}_{\text{H}_2\text{O}}}. \quad (7)$$

336 Conversely, the mass fraction of water is  $\tilde{f}_{\text{H}_2\text{O}} = 1 - \tilde{f}_{\text{NH}_3}$ .

337 The collection efficiency depends on (1) how ice particles follow the flow around  
 338 the mushball and (2) how effectively they remain bound upon collision. The first  
 339 parameter is directly linked to the Stokes parameter of the ice particles, i.e., the  
 340 ratio of their stopping time to the mushball-crossing time  $v_{\text{fall}}/\tilde{d}$ . For the ice parti-  
 341 cles that we consider, we are in the Stokes regime, implying a Stokes number  $St \sim$   
 342  $\tilde{\rho}_{\text{particle}}\tilde{s}_{\text{particle}}^2 v_{\text{fall}} / (18\eta_a \tilde{d})$ , where  $\tilde{\rho}_{\text{particle}}$  and  $\tilde{s}_{\text{particle}}$  are the particle physical den-  
 343 sity and size, respectively (Kundu & Cohen, 2016). For  $\tilde{\rho}_{\text{particle}} = 0.3\text{g}\cdot\text{cm}^{-3}$  and  
 344  $\tilde{s}_{\text{particle}} = 100\ \mu\text{m}$ , and using the approximation that  $C_d = 0.6$  for mushballs in the 0.1  
 345 to 5 cm size range, we obtain  $St \sim 100(\tilde{d}/1\text{cm})^{1/2}$  implying that hydrodynamic effects  
 346 should not decrease the collection efficiency (Homann et al., 2016).

347 The second parameter, the collection efficiency  $E$ , is difficult to estimate. In the  
 348 Earths atmosphere, its value for collisions between ice particles ranges between unity  
 349 to less than 0.1 (Phillips et al., 2015). Being at or close to the melting temperature is a  
 350 key feature of the ability of particles to stick. Extrapolating these results to the Jupiter  
 351 case, we thus expect  $E \sim 1$  when thermodynamic conditions predict the presence of  
 352 liquid NH<sub>3</sub>·H<sub>2</sub>O and a smaller value away from that regime. For simplicity, we assume  
 353 that  $E = 0.3$  in the regime where the only condensates are made of H<sub>2</sub>O ice and  $E = 1$   
 354 elsewhere.

### 355 3.3 Evaporation of mushballs

356 As mushballs fall into a high-enough temperature region, they will begin to melt  
 357 and evaporate. In order to account for this process, we use the approach derived for  
 358 the melting of hail on Earth (Pruppacher & Klett, 1997). The rate at which hail  
 359 melts is controlled by heat conduction from the atmosphere into the hailstone, the  
 360 development of an interface between liquid water and solid ice inside the hail stone  
 361 and the shedding of the water shell due to hydrodynamic instabilities. The hailstone is  
 362 kept cooler than the surrounding atmosphere due to latent heat release by evaporation.

363 The evolution of the hailstone structure upon melting can be relatively complex:  
 364 a water torus generally forms and shedding of either small or large drops can take  
 365 place. Depending on the hailstone size, this can take place either continuously or  
 366 intermittently. At mm sizes, an eccentric melting of the ice core takes place (Rasmussen  
 367 et al., 1984).

368 Here, we use a simplified approach that considers that shedding takes place  
 369 instantaneously. In that case the hailstone is kept near its melting temperature  $\tilde{T}_0 \sim$

370 0°C and its size is governed by the following equation (Pruppacher & Klett, 1997):

$$\frac{da}{dt} = \frac{1}{(L_m + \tilde{c}_{P,H_2O}\Delta\tilde{T})\rho_i a} \left[ -k_a (T - \tilde{T}_0) f_h + D_{H_2O} \frac{\mu_v L_v}{\mathcal{R}} \left( \frac{P_{\text{sat}}(\tilde{T}_0)}{\tilde{T}_0} - H_a \frac{P_{\text{sat}}(T)}{T} \right) f_v \right], \quad (8)$$

371 where  $f_h$  and  $f_v$  are ventilation coefficients for heat and vapor, respectively, and are  
372 measured experimentally to be

$$\begin{aligned} f_h &= \frac{\chi}{2} N_{\text{Re}}^{1/2} \left( \frac{\nu_a}{K_a} \right)^{1/3} \\ f_v &= \frac{\chi}{2} N_{\text{Re}}^{1/2} \left( \frac{\nu_a}{D_{H_2O}} \right)^{1/3} \end{aligned} \quad (9)$$

373 The following quantities have been used:  $L_m$  and  $L_v$  are the latent heat of melting and  
374 vaporization, respectively (accounting for their temperature dependence, but assuming  
375 pure  $H_2O$ ),  $k_a$  is the thermal conductivity of the atmosphere,  $\nu_a$  its kinematic viscosity,  
376  $K_a = k_a/(\rho c_P)$  its thermal diffusivity,  $D_{H_2O}$  the diffusivity of water vapor in the  
377 atmosphere,  $P_{\text{sat}}$  the saturation pressure,  $H_a$  the relative humidity of the atmosphere,  
378  $N_{\text{Re}}$  is the Reynolds number defined in the terminal velocity section, and  $\chi$  is a mass  
379 transfer coefficient of order unity. Given the extended fall, we account for the internal  
380 temperature change of the hailstone, with  $\tilde{c}_{P,H_2O}$  being the specific heat and  $\Delta\tilde{T} =$   
381  $\tilde{T}_i - \tilde{T}_0$  the difference between an internal temperature  $\tilde{T}_i$  and that at the surface  $\tilde{T}_0$ .

382 Given the large Reynolds number ( $10^3$  to  $10^6$ ) considered here, the ventilation  
383 coefficients are large and represent the largest effect governing the melting of the  
384 hailstone. The Prandtl and Schmidt numbers that enter these coefficients are close to  
385 unity: As seen from Table B1,  $(\nu_a/K_a)^{1/3} \sim 0.88$  and  $(\nu_a/D_{H_2O})^{1/3} \sim 1.05$  so that to  
386 first approximation  $f_h \sim f_v$ . Experiments suggest that  $\chi \sim 0.76$  (Pruppacher & Klett,  
387 1997). Overall, this yields  $f_h \sim f_v \sim 10$  to 400. We note that this scaling law should  
388 change in the super-critical regime ( $N_{\text{Re}} \gtrsim 3 \times 10^5$ ), but it is not even clear whether  
389 melting should be increased or decreased over this relation. Dedicated experiments  
390 should be conducted in order to determine more precisely the mushball evaporation  
391 level.

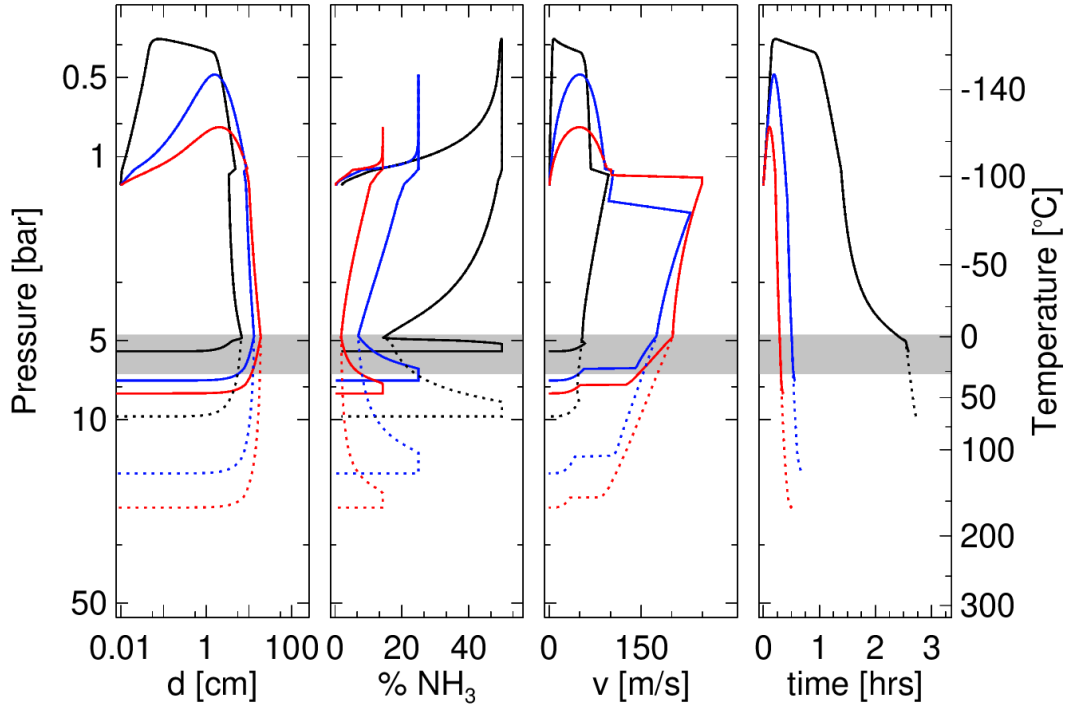
392 Although most of the complex processes observed during hailstone melting are  
393 not included, Appendix A shows that the approach does reproduce relatively well obser-  
394 vations in the Earths atmosphere and in wind tunnels. It also shows that additional  
395 heating due to viscous drag can be neglected.

### 396 3.4 The rise and fall of mushballs in Jupiters atmosphere

397 We now apply our model for growth and evaporation of mushballs to the case  
398 of Jupiter. We are interested in situations where storms are able to reach the upper  
399 regions of the atmosphere (above the 1 bar pressure level). This corresponds to large  
400 storms. We thus assume an updraft velocity of 50 m/s generated from the cloud-base  
401 level and extending to the 0.4-bar level (Hueso et al., 2002; Sugiyama et al., 2014). We  
402 assume that the upward velocity goes to zero away from that pressure range gradually  
403 with an error function:

$$v_{\text{up}} = v_0 \left\{ 1 - \text{erf} \left[ \max \left( 0, -\frac{\log_{10} \left( \frac{P}{P_{\text{top}}} \right)}{\delta_P} \right) \right] \right\} \left\{ 1 - \text{erf} \left[ \max \left( 0, \frac{\log_{10} \left( \frac{P}{P_{\text{bottom}}} \right)}{\delta_P} \right) \right] \right\}, \quad (10)$$

404 and we choose  $P_{\text{top}} = 0.4$  bar,  $P_{\text{bottom}} = 5$  bar and  $\delta_P = 0.05$ . (The precise values are  
405 not important, as long as the updraft takes place at pressures between say, 0.5 and 1.5  
406 bar).



**Figure 3.** Characteristics of hail/mushballs as a function of pressure in Jupiter, for three values of the abundance of water-ice particles in the upper atmosphere: 100 ppmv (black), 600 ppmv (blue), and 1200 ppmv (red), assuming an updraft velocity of 50 m/s (see text). The first panel shows the diameter of hailstones, the second one the percentage of  $\text{NH}_3$  molecules that they contain, the third one their terminal velocity and the fourth one the time spent since their formation. The dotted lines correspond to cases in which the ventilation factor has been decreased by a factor 10 compared to the nominal value (see text). The temperatures in Jupiters atmosphere are indicated on the right. The grey area corresponds to the location of the water cloud base, i.e. between 4.8 bar and 6.7 bar according to the Juno measurements (Li et al., 2020).

407 Based on terrestrial data showing that graupels and ice crystals have densities  
 408 ranging from 0.05 to 0.9  $\text{g/cm}^3$  (Pruppacher & Klett, 1997), we adopt a physical  
 409 density both for  $\text{H}_2\text{O}$  ice and for  $\text{H}_2\text{O}\cdot\text{NH}_3$  ice of 0.3  $\text{g/cm}^3$ . In the region where  
 410  $\text{H}_2\text{O}\cdot\text{NH}_3$  liquid forms we assume that the collected ice have a density of 0.9  $\text{g/cm}^3$ .  
 411 In that region, we also assume that the mushball melts partially to an overall density  
 412 of 0.9  $\text{g/cm}^3$ .

413 We use the following values of the physical parameters, evaluated at 300K which  
 414 corresponds approximately to the atmospheric temperature where mushballs melt: for  
 415 water ice,  $c_P = 2.0 \times 10^7 \text{ erg g}^{-1} \text{ K}^{-1}$ ,  $L_m = 3.34 \times 10^9 \text{ erg g}^{-1}$ ; for water vapor,  
 416  $L_v = 2.515 \times 10^{10} \text{ erg g}^{-1}$ ,  $D_{\text{H}_2\text{O}} = 0.17 \text{ cm}^2 \text{ s}^{-1}$ ,  $\mu_v = 18$ ; for hydrogen,  $k_a = 1.85 \times$   
 417  $10^4 \text{ erg s}^{-1} \text{ cm}^{-1} \text{ K}^{-1}$ . We further assume that  $H_a = 1$ , except below the cloud base,  
 418 assumed to be at 5.8 bar, corresponding to an enrichment of water equal to 2.7 times  
 419 the protosolar value (Li et al., 2020). (As shown in Appendix A3, this assumption has  
 420 negligible consequences for the outcome of the model.)

421 We use a temperature profile that is based on the Galileo probe measurements  
 422 (Seiff et al., 1998) and extended below 22 bars using an adiabatic profile derived from  
 423 an interior model of Jupiter (Guillot et al., 2018).

Figure 3 shows the resulting evolution of mushballs for three cases: Global abundances of water ice carried above the 1-bar level of 100 ppmv, 600 ppmv and 1200 ppmv, respectively. The simulation starts when water-ice particles generated at depth by the storm and carried in the updraft reach the 1.5-bar level. We start from an initial seed of 100  $\mu\text{m}$  that melts due to  $\text{NH}_3$  adsorption, starts collecting  $\text{H}_2\text{O}\cdot\text{NH}_3$  liquid and, for the 600ppmv and 1200ppmv water-ice cases,  $\text{H}_2\text{O}$  ice particles. Its terminal velocity is small compared to the updraft velocity. When reaching the 1-bar region, the particle accretes solid  $\text{H}_2\text{O}\cdot\text{NH}_3$  and  $\text{H}_2\text{O}$  ice. It continues to ascend until it has grown to a point where its terminal velocity equals the updraft velocity. At this point, it will start to fall, scavenging more particles on the way.

Between 1.1 and 1.5 bar, the mushball crosses again the liquid  $\text{H}_2\text{O}\cdot\text{NH}_3$  region and partially melts. The density change (to about  $\sim 0.9 \text{ g}\cdot\text{cm}^{-3}$ ) yields an increase of the Reynolds number. For the middle and high ice abundance case, it becomes supercritical which yields a very significant increase of the terminal velocity to about 300 m/s. (In the low-abundance case, the density change is not sufficient and the velocity stays confined to  $\sim 100\text{m/s}$ ).

In this same range of pressures, the scavenging of  $\text{H}_2\text{O}$  ice leads to a progressive increase of the  $\text{H}_2\text{O}$  mass in the mushball. The fraction of  $\text{NH}_3$  decreases to a minimum of 3% in the high water-ice case to 20% in the low water-ice case. At that point, the temperature has reached  $0^\circ\text{C}$ , the water-ice melting point, which leads to a progressive melting of the outer shell of the mushball. The  $\text{NH}_3$  fraction thus increases up to the value it had after crossing the liquid  $\text{H}_2\text{O}\cdot\text{NH}_3$  region. The last phase is a very quick melting and evaporation of the mushball, at pressures of 6.3 bar, 8.1 bar, and 9.6 bar for the low, medium and high water-ice cases, respectively. If we decrease the ventilation factor by an order of magnitude (to account for possible changes of the empirical relation at high Reynolds number), the mushballs penetrate deeper, i.e., to 10, 17 and 24 bar, respectively (see Fig. 3).

We find the depth at which mushballs evaporate to be insensitive to our choice of the drag coefficient  $C_d$  for supercritical Reynolds numbers due to a balance between shorter timescales and larger ventilation coefficients. However, the time taken for mushballs to reach the evaporation level is proportional to  $\sqrt{C_d}$  and is thus correspondingly shorter due to the supercritical Reynolds number effect.

We can derive several important conclusions from this relatively simple model: The first one is that during strong storms, ammonia can be efficiently carried from the top of Jupiters atmosphere down to levels *below* the water-cloud base. This is the case at least for the medium and high water-ice abundances. Equally significantly, for a number of cases,  $\text{NH}_3$  is carried below the water cloud base more efficiently than  $\text{H}_2\text{O}$ , i.e.,  $\tilde{f}_{\text{NH}_3}/\tilde{f}_{\text{H}_2\text{O}} > (N/O)_\odot = 0.135$ , or equivalently  $\tilde{f}_{\text{NH}_3} > 0.117$ , where  $(N/O)_\odot$  is the protosolar nitrogen to oxygen mixing ratio (Lodders, 2003). This implies that the downward transport of ammonia by water storms is efficient and can lead to a depletion of the upper atmosphere ammonia.

An exploration of the sensitivity to the parameters of the model is presented in Appendix A3. The depth of penetration of mushballs extends from 5.1 to 31 bar, depending on parameter values (quantity of water ice, updraft velocity, sticking efficiency...etc.). The cases for which water ice evaporate mostly above the water cloud base and the mushball core is deposited below appear most favorable. In that case, evaporated water may be recycled into storms while the aqueous ammonia mixture at the core of the mushballs would then be able to form evaporative downdrafts below the cloud base. Storms with updraft velocities between 10 and 50 m/s and between 100 and 600 ppmv of water ice carried to the 1.5 bar region therefore seem most promising to account for the Juno data.

Of course, we must add several important caveats. Compared to models of hail formation on Earth, this one is extremely simplified. In particular, it does not include complex geometrical effects inherent to hailstorm formation on Earth, the effect of turbulence within the cloud, the combined growth of a population of particles, and feedbacks due to evaporative cooling. On the other hand it does show that a simple model can already account for the formation of  $\sim 10$ -cm mushball hail in Jupiter. When putting Earth and Jupiter in perspective, we note that Earth can form large hailstones (up to 0.77 kg see e.g. Roos 1972), that this requires strong updrafts ( $\sim 50$  m/s) and the presence of liquid water droplets that are supercooled to around  $-15^\circ\text{C}$  (Pruppacher & Klett, 1997), a relatively rare occurrence. Jupiter has equivalently strong updrafts (Stoker, 1986; Gierasch et al., 2000; Hueso et al., 2002; Sugiyama et al., 2014), and the presence of a liquid phase in contact with solids is guaranteed as long as ice particles are carried at least to the 1.5-bar level (which occurs only for storms with already large upward velocities). Two important differences are that on Jupiter large storms (characterized by large updraft velocities  $> 10$  m/s at 2 bars) should always be able to loft ice particles to the 1.1- to 1.5-bar region where melting occurs, that the range of altitudes over which growth by scavenging can take place is vastly larger ( $\sim 50$  km in Jupiter versus  $\sim 3$  km on Earth). This points to a hail formation mechanism on Jupiter that should be significantly more efficient than on Earth.

### 3.5 Internal evolution of mushballs

Figure 4 examines the evolution of the internal structure of the mushballs. We identify six evolution phases:








- Phase 1: Early adsorption of  $\text{NH}_3$  into an  $\text{H}_2\text{O}$  ice crystal, its melting and subsequent growth. For high enough abundances of  $\text{H}_2\text{O}$  ice, the melting should be partial, i.e. a relatively high-density slush should form.
- Phase 2: Growth by accretion of low-temperature, porous ices ( $\text{H}_2\text{O}\cdot\text{NH}_3$  and  $\text{H}_2\text{O}$ ).
- Phase 3: Partial melting of the mushball with continuous accretion of  $\text{H}_2\text{O}$  ice.
- Phase 4: Accretion of low-density  $\text{H}_2\text{O}$  ice crystals.
- Phase 5: Melting of the outer  $\text{H}_2\text{O}$  shell and shedding. The size and mass decrease.
- Phase 6: Evaporation of the  $\text{H}_2\text{O}\cdot\text{NH}_3$  core.

The buildup of an  $\text{H}_2\text{O}$  ice shell in phase 3 is critical because it isolates the liquid core of the mushball thermally and prevents  $\text{NH}_3$  from diffusing out and be lost to the atmosphere. Even though the ice crystals collected should be very porous, the part of the  $\text{H}_2\text{O}$  ice shell in contact with the  $\text{H}_2\text{O}\cdot\text{NH}_3$  liquid is expected to be compact due to its interaction with the liquid.

Thermal equilibration within the mushball takes place with a characteristic time of order  $\tau \approx d^2/\alpha_i$  where  $\alpha_i \sim 2.2 \times 10^{-2} \text{ cm}^2 \text{ s}^{-1}$  is the thermal diffusivity of  $\text{H}_2\text{O}$  ice. It is thus approximately only 45 seconds for a 1 cm mushball but 1.3 hours for a 10 cm one. For comparison, the examples shown in Fig. 3 correspond to falltimes of  $\sim 40$  min from 1.5 to 5 bar for the 100 ppmv  $\text{H}_2\text{O}$  abundance case and only about 5 min from 1.5 to about 10 bar for the two other cases. Thermal equilibration will lead to a progressive melting of the  $\text{H}_2\text{O}$  ice crust of the mushball from the inside-out and a decrease of the ammonia concentration in the mushball core. It could lead to a sudden break-up of the mushball when the  $\text{H}_2\text{O}$  crust becomes too thin. This effect should be examined but should not affect our conclusions qualitatively.

Similarly, diffusion of ammonia through the solid-ice crust is expected to be slow. The diffusion coefficient for ammonia in water ice measured experimentally at 142 K



Phase	Morphology	Size	Pressure	Comments
0		10-100 $\mu\text{m}$	4.5-1.1 bar	H <sub>2</sub> O ice crystal
1		100 $\mu\text{m}$ -1mm	1.5-1.1 bar	H <sub>2</sub> O · NH <sub>3</sub> liquid + H <sub>2</sub> O ice slush
2		1mm-5cm	1.1-0.5 bar	H <sub>2</sub> O · NH <sub>3</sub> liquid core surrounded by shell of low density H <sub>2</sub> O · NH <sub>3</sub> ice and H <sub>2</sub> O ice
3		2-3cm	1.1-1.5 bar	H <sub>2</sub> O · NH <sub>3</sub> liquid core surrounded by H <sub>2</sub> O ice shell
4		3-10cm	1.5-5 bar	H <sub>2</sub> O · NH <sub>3</sub> liquid core surrounded by H <sub>2</sub> O ice shell (possibly porous away from the core)
5		10-2cm	5-10 bar	H <sub>2</sub> O · NH <sub>3</sub> liquid core H <sub>2</sub> O ice crust H <sub>2</sub> O water shell
6		2-0cm	7-11 bar	Evaporating H <sub>2</sub> O · NH <sub>3</sub> liquid droplet

**Figure 4.** The phases and internal structure of mushballs.

525 is  $\tilde{D}_{\text{NH}_3}^{\text{sol}} \sim 4 \times 10^{-10} \text{ cm}^2/\text{s}$  (Livingston et al., 2002). This may be extrapolated to  
 526 be up to 2 orders of magnitude higher at  $\sim 250 \text{ K}$ , based on Na which has a similar  
 527 behavior (Livingston et al., 2002). Thus, using the same approach as in Section 2.2,  
 528 we expect ammonia to diffuse outward only by about  $\sim 100 \mu\text{m}$  in one hour, i.e., a  
 529 negligible amount given that we expect  $\sim \text{cm}$  sizes for the mushballs.

530 Importantly, the highly concentrated ammonia-water mush at the center would  
 531 be delivered last in Jupiter's deep atmosphere. Some of the water that is evaporated  
 532 at higher levels can thus be recycled to power new storms and lead to the formation  
 533 of more mushballs.

#### 534 4 Importance of evaporative downdrafts

535 For our nominal ventilation coefficient, the evaporation of mushballs occurs near  
 536 10 bars, a pressure level that is not sufficiently deep to account for abundance increase  
 537 inferred from the Juno MWR data (Bolton et al., 2017; Li et al., 2017). One possibility  
 538 is that ventilation coefficients in the super-critical regime are decreased. However an  
 539 other mechanism, the presence of evaporative downdrafts, must lead to further sinking  
 540 of ammonia (and water).

541 On Earth, any rain, snow or hail accumulates on the surface. In Jupiter, the  
 542 absence of such a surface implies that a pocket of gas with an increased concentration  
 543 of ammonia and water must form. It is difficult to estimate precisely the concentration  
 544 increase because it depends on geometrical factors and the time evolution of the storm.  
 545 But we estimate that it may be substantial. Let us assume a storm surface area  $\sigma_{\text{storm}}$ ,  
 546 an updraft velocity  $v_{\text{up}}$  for a typical characteristic timescale  $\Delta t$ . The mushballs evap-

orate lower than the cloud base, in an area  $\sigma_{\text{down}}$  and down on to a depth  $H_{\text{down}}$ . The typical densities are  $\rho_{\text{storm}} \sim 5 \times 10^{-4} \text{ g cm}^{-3}$  around 5 bar and  $\rho_{\text{down}} \sim 2 \times 10^{-3} \text{ g/cm}^3$  around 30 bar. The enrichment (i.e. fractional increase of the mixing ratio of water and ammonia) is of order  $\Delta x \sim \epsilon x (\sigma_{\text{storm}}/\sigma_{\text{down}}) (\rho_{\text{storm}}/\rho_{\text{down}}) (v_{\text{up}} \Delta t / H_{\text{down}})$ . The first term in parenthesis is of order unity, the second one is  $\sim 1/6$ . The Voyager storm analyzed by Hueso et al. (2002) took about 10 days to develop and seemed relatively well fixed in latitude and longitude (on the local differential rotation frame). We hence estimate that  $H_{\text{down}} \sim 100 \text{ km}$ ,  $v_{\text{up}} \sim 50 \text{ m/s}$  and  $\Delta t \sim 3 \text{ hrs}$ . The last term in parenthesis is thus  $v_{\text{up}} \Delta t / H_{\text{down}} \sim 5$ . With an assumed mushball formation rate  $\epsilon \sim 0.3$  we thus get  $\Delta x / x \sim 0.25$ . This is of course only an order of magnitude estimate and could vary significantly depending on the storm geometry and velocity. It is likely that localized bubbles that are highly enriched in water and ammonia will form and be only weakly affected by turbulence, thus effectively increasing  $\Delta x$  much above that value.

In fact, even a modest enrichment can power strong downdrafts: For a perfect gas with a volume mixing ratio of vapor  $x$ , with  $\zeta = \mu_v / \mu_d$  being the ratio of the mean molecular mass of vapor to that of dry gas

$$\rho = [1 + (\zeta - 1)x] \frac{\mu_d P}{RT}. \quad (11)$$

Evaporation of water (and ammonia) will result in an increase of mean molecular weight (due to the addition of vapor) and a cooling by evaporation, leading to a density increase

$$\frac{\Delta \rho}{\rho} \approx (\zeta - 1) \Delta x - \frac{\Delta T}{T}, \quad (12)$$

where we assumed  $x \ll 1$ . The change in temperature due to evaporation is  $\Delta T = L_v \zeta \Delta x / c_P$ , where  $L_v$  is the latent heat of vaporization per unit mass of condensate (water) and  $c_P$  is the heat capacity per unit mass of atmosphere. Thus we can rewrite the density change as a function of the increase in vapor mixing ratio

$$\frac{\Delta \rho}{\rho} \approx \left( \zeta - 1 + \frac{L_v \zeta}{c_P T} \right) \Delta x. \quad (13)$$

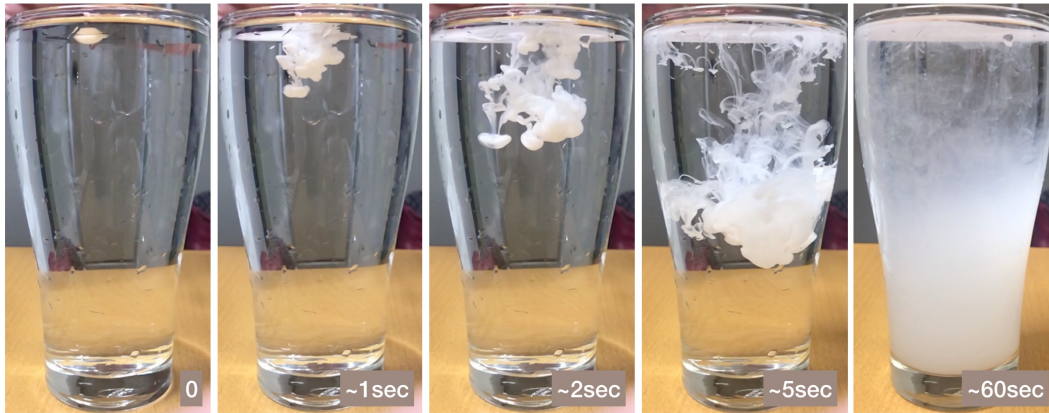
For our conditions we get  $\zeta - 1 \approx 6.8$  and  $L_v \zeta / c_P T \approx 4.7$ , i.e. the increase in mean molecular weight dominates slightly over the effect of evaporating cooling.

An estimate of the downdraft velocity can be obtained by calculating the work of the buoyancy force over a depth  $\ell$  and by equating half of this work to the kinetic energy. This implies

$$v_{\text{down}} \approx \left( g \frac{\Delta \rho}{\rho} \ell \right)^{1/2}. \quad (14)$$

For a length equal to the pressure scale height  $\ell \sim H_P \sim 30 \text{ km}$ , and Jupiter's gravity, we get  $v_{\text{down}} \approx 100 (\Delta x / 10^{-3})^{1/2} \text{ m/s}$ . For comparison, (Sugiyama et al., 2014) obtain downdrafts reaching about 50 m/s. We point out that downdrafts have been recognized to be an essential part of the Sun's convection (Stein & Nordlund, 1998). In Jupiter, downdrafts are powered both by evaporative cooling and by molecular weight effects and should play an even more prominent role (Ingersoll et al., 2017).

Figure 5 illustrates what might be occurring in Jupiter with a simple experiment. Milk and water are fully miscible, like ammonia and water with hydrogen below the water cloud base in Jupiter. But when adding a spoonful of milk in the glass of water, instead of slowly diffusing in the glass, it rapidly sinks to the bottom through "milk plumes". These result from Rayleigh-Taylor instabilities which are of course well known in hydrodynamics (see e.g., Turner (1969)). Here, our purpose is to illustrate the fact that this process, while of minor importance in the Earth atmosphere (moist air is slightly lighter than dry air at the same temperature), is likely to play a crucial role in Jupiter. (Of course, our water and milk experiment is strongly affected by wall



**Figure 5.** Simple experiment to illustrate the importance of localized downdrafts in fluid mixtures. Here, at  $t=0$ , a tea spoon of fat milk from the refrigerator ( $\sim 10^\circ\text{C}$ ) is added to a glass of water at room temperature ( $\sim 20^\circ\text{C}$ ). Although the milk would be able to dissolve homogeneously in the glass, its slightly higher density resulting from its higher mean molecular weight and lower temperature yields strongly localized downdrafts. The final state is characterized by a gradient of increasing milk concentration with depth. Similarly, we expect strong storms in Jupiter to deliver to about 10 bar a cold and relatively highly concentrated water- and ammonia-rich gas leading to downdrafts able to reach the deeper levels of the planets. Individual storms should have horizontal extents of about  $\sim 25$  km (Hueso et al., 2002) and Juno measurements indicate that ammonia concentration increases on a vertical scale of at least 100 km. Although this is largely coincidental, we note that the geometry for that simple experiment is relatively similar to that in Jupiter.

590 effects and cannot be used to infer the depth of the plumes. In Jupiter, compression  
 591 effects, turbulence and horizontal mixing are factors that should all be taken into  
 592 account to infer the possible vertical extent of these downdrafts.) Unfortunately, its  
 593 modelling and proper inclusion into global atmospheric models is notoriously difficult  
 594 because of the variety of scales involved.

595 We also note that collective effects may play a role in leading to a further sinking  
 596 of the condensates (water and ammonia) in Jupiter: In mushball regions, the tem-  
 597 peratures should be locally cooler by  $\delta T/T \approx -4.7\Delta x$ . We have estimated for the  
 598 whole column that  $\Delta x \approx 0.25x$ , i.e., a quantity of order  $10^{-3}$ . But it is likely that  
 599 in some regions, this value is much larger than that, in which case the evaporation  
 600 would be delayed by the low temperature of the downwelling plume. For example if  
 601  $\Delta x \sim 10^{-2}$ , at the 10 bar pressure level where the temperature should be  $65^\circ\text{C}$ , it  
 602 would be locally depressed to  $50^\circ\text{C}$ , corresponding to an increased sinking by  $\sim 8$  km.  
 603 Furthermore, the formation of a downdraft also means a faster downward transport of  
 604 the mushballs with delayed evaporation. Detailed hydrodynamical simulations should  
 605 be conducted in order to estimate the depth to which ammonia- and water-rich bubbles  
 606 can be transported to.

607 Last but not least, we note that for the sinking to stop, the surrounding vapor  
 608 mixing ratio must increase with depth so that the buoyancy force reverses. The location  
 609 and magnitude of this increase will depend on local turbulence, entrainment of gas  
 610 both in updrafts and downdrafts; on the radiative cooling of the plumes and on global  
 611 horizontal mixing. This problem is beyond the scope of the present work, but it is  
 612 likely to have deep consequences for our understanding of the interior structure of the  
 613 planet.

## 614 5 Conclusion

615 The variability of ammonia's concentration as a function of latitude and to great  
 616 depths in Jupiter's deep atmosphere (Bolton et al., 2017; Li et al., 2017) is one of the  
 617 most important surprises of the Juno mission and remains thus far unaccounted for.  
 618 We have shown that thermoequilibrium chemical calculations predict the existence of  
 619 a low-temperature region in which ammonia and water can form a liquid mixture with  
 620 a high ( $\sim 1/3$ ) concentration of ammonia. This region is located between 1.1 and 1.5  
 621 bar and temperatures between 173 K and 188 K. Jupiter's powerful storms can deliver  
 622 water-ice crystals to that region. We have shown that ammonia vapor can dissolve into  
 623 the ice crystals to form a high viscosity liquid ammonia-water 'mush', on timescales of  
 624 minutes to tens of minutes. The increased mass and density of the particles thus formed  
 625 increases differential velocities and the presence of liquid is expected to also lead to a  
 626 high sticking efficiency, two factors which are crucial for the growth of hail-like particles  
 627 that we call 'mushballs'. We have presented a simple model to account for their growth,  
 628 their fall to the deep atmosphere and their evaporation. Depending on the amount of  
 629 water-ice particles lofted by the storms, and depending on the poorly known ventilation  
 630 coefficients governing heat conduction efficiency from the atmosphere to the mushballs,  
 631 they should reach pressure levels of 5 bars and even as deep as 27 bars. Further sinking  
 632 is warranted by the fact that the evaporated mushballs both have a high molecular  
 633 weight and low temperature.

634 The fact that the cores of the mushballs contain a mixture that is highly concen-  
 635 trated in ammonia and the fact that this core is the last to be evaporated provides a  
 636 potential mechanism to explain the ammonia depletion in a large fraction of Jupiter's  
 637 atmosphere. Their evaporation deeper than the water cloud level and their further  
 638 transport by downdrafts can potentially explain the great depth to which ammonia  
 639 depletion is observed by Juno. We note (i) that since ammonia is at the center of the  
 640 mushballs, it is delivered last, (ii) that  $\text{H}_2\text{O}$  that evaporated on the way can be reused

in other thunderstorms and therefore cycles further ammonia depletion, (iii) that the  $\text{NH}_3/\text{H}_2\text{O}$  concentration at the center of mushballs is  $\sim 0.3$ , much greater than the solar N/O ratio of 0.1320, implying that the mechanism is efficient. We also note that the minimum in the derived  $\text{NH}_3$  abundances (Bolton et al., 2017; Li et al., 2017) is very close to the minimum  $\text{NH}_3$  abundance below which the mushball mechanism cannot work (i.e., from Fig. 1, a partial pressure  $P_{\text{NH}_3} \sim 10^{-4}$  bar, corresponding to a  $\sim 100$  ppmv  $\text{NH}_3$  mole fraction in Jupiter). Finally, recent Juno observations in the optical show lightning flashes that are formed between 1 and 2 bar, consistent with the presence of liquid  $\text{NH}_3\text{-H}_2\text{O}$  and large particles in the mushball formation region (Becker et al., 2020). In a subsequent paper, we develop a model of Jupiter's deep atmosphere to attempt to reproduce the dominant features of Juno's observations.

## Appendix A Evaporation of hail

### A1 Application to the Earth case

We apply our simple model for the evaporation of hailstones and mushballs (Eqs. 8, 9) to the case of the Earth atmosphere, based on the work of Rasmussen and Heymsfield (1987). We assume the Earth gravity,  $g = 981 \text{ cm/s}^2$ , and extremely simplified model reproducing the case of Rasmussen and Heymsfield (1987), from altitude  $z = 0.8 \text{ km}$  to  $z = 5.2 \text{ km}$ , pressure from 0.9 to 0.6 bar, temperature from  $24^\circ\text{C}$  to  $0^\circ\text{C}$  and a relative humidity between 60% to 100% at the highest altitude where the hail originates. The mean molar weight of air is  $\mu = 29$ , its thermal conductivity  $k_a = 2570 \text{ erg s}^{-1} \text{ cm}^{-1} \text{ K}^{-1}$ , its dynamic viscosity  $\eta = 1.8 \times 10^{-4} \text{ g cm}^{-1} \text{ s}^{-1}$  and the diffusivity of water in air,  $0.3 \text{ cm}^2/\text{s}$ . The other parameters are the same as for Jupiter.

Figure A1 compares observational data and theoretical tracks (Rasmussen & Heymsfield, 1987) to results of our model calculated with Eqs. (8) and (9). Some differences are visible but they are small compared to other uncertainties in the model.

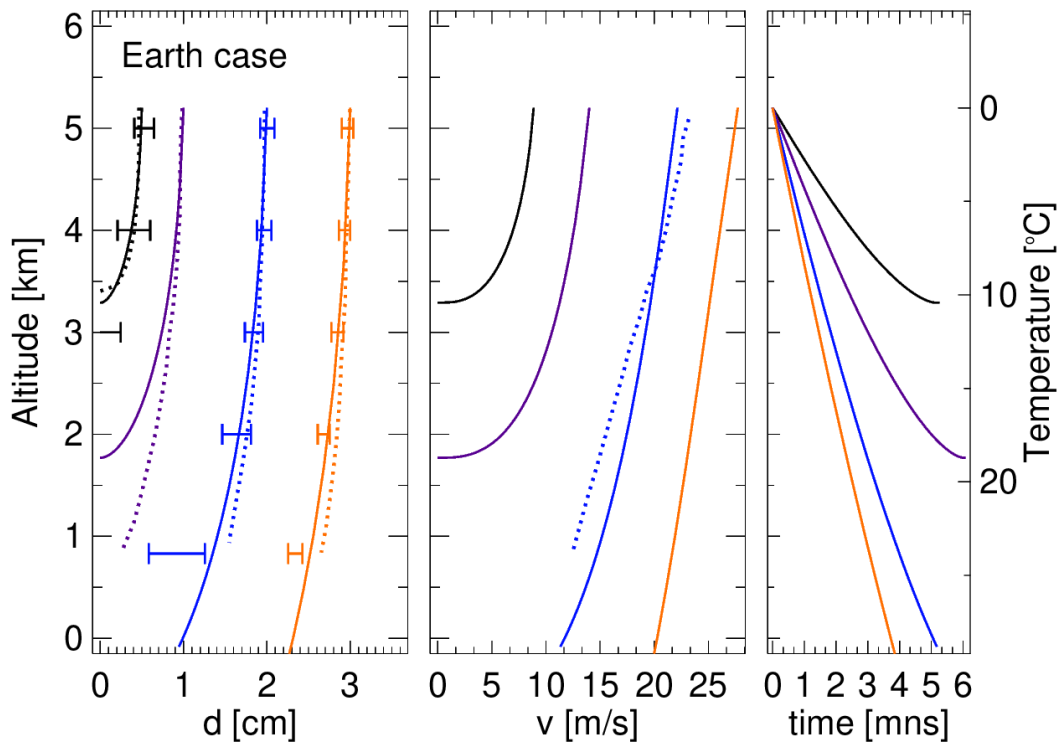
### A2 Effect of drag heating

In the case of Jupiter, the high fall speed of mushballs raises the question of whether drag friction (not included in Eq. 8) may lead to an even faster evaporation. This can be estimated as follows: Assuming an approximate constant terminal velocity, the energy dissipated per time  $\Delta t$  by drag is  $\Delta E \sim \tilde{M} g v_{\text{fall}} \Delta t$ . Because the size considered is much smaller than the mean free path, this energy is dissipated in the gas and can then potentially heat the mushball. The part that is of interest to us is the fraction  $\epsilon_{\text{drag}}$  that is dissipated in the boundary layer around the mushball, which has a thickness  $\ell \sim \sqrt{K_a d / v_{\text{fall}}}$ . With  $K_a \sim 0.3 \text{ cm}^2/\text{s}$ ,  $d \sim 10 \text{ cm}$  and  $v_{\text{fall}} \sim 300 \text{ m/s}$ , we obtain  $\ell \sim 0.01 \text{ cm}$ . The gas in the boundary layer of volume  $V \sim \pi d^2 \ell$  is replaced at a rate  $\Delta t \sim d / v_{\text{fall}}$ , implying a change of temperature in the gas

$$\Delta T \sim \epsilon_{\text{drag}} \frac{\Delta E}{c_{P,a} \rho_a V} \sim \epsilon_{\text{drag}} \frac{1}{6} \frac{\tilde{\rho}_{\text{ice}}}{\rho_a} \frac{g d^2}{c_{P,a} \ell}.$$

With  $g = 2600 \text{ cm s}^{-2}$ ,  $\tilde{\rho}_{\text{ice}} = 0.9 \text{ g/cm}^3$ ,  $\rho_a = 3 \times 10^{-4} \text{ g cm}^{-3}$  and  $c_{P,a} = 1.4 \times 10^8 \text{ erg g}^{-1} \text{ K}^{-1}$ , we obtain  $\Delta T \sim \epsilon_{\text{drag}} \times 30 \text{ K}$ .

In order to estimate  $\epsilon_{\text{drag}}$ , let us consider the case of a human skydiver on Earth, falling at a terminal velocity around 50 m/s. With a weight of 75 kg and a density of  $\tilde{\rho} = 1 \text{ g/cm}^3$ , we consider that  $d \approx 50 \text{ cm}$ . Using parameters for the Earth at sea level,  $K_a \sim 0.19 \text{ cm}^2/\text{s}$ ,  $g = 981 \text{ cm/s}^2$ ,  $\rho_a = 1.2 \times 10^{-3} \text{ g/cm}^3$  and  $c_{P,a} = 1.0 \times 10^7 \text{ erg/(g K)}$ , we obtain  $\ell \sim 0.04 \text{ cm}$  and  $\Delta T \sim \epsilon_{\text{drag}} \times 850 \text{ K}$ . Everyday experience does tell us that the heating should be less than a few Kelvin (the same could be applied to e.g. driving a car on the highway). Therefore  $\epsilon_{\text{drag}} < 10^{-2}$ , yielding a temperature increase which is negligible compared to other uncertainties.



**Figure A1.** Comparison of the evolution of hailstones obtained from wind tunnel experiments (horizontal error bars), dedicated calculations (Rasmussen & Heymsfield, 1987) (dotted curves) and our simple model (plain lines). The three panels show the evolution with altitude of the hailstone diameter (left), terminal velocity (center) and time (right). The colored lines correspond to different initial diameters: 0.5 cm (black), 1 cm (purple), 2 cm (blue) and 3 cm (orange).



Another way to see this is as follows: The temperature increase in the boundary layer across the mushball is proportional to gravity (2.6 times higher in Jupiter), but is inversely proportional to the product of gas density and heat capacity. At 1 bar in Jupiter, this product is similar to that at sea level on the Earth, but deeper in Jupiter, where mushballs evaporate, it is an order of magnitude higher. Therefore, the increase in temperature in the boundary layer is expected to be smaller than for a similar situation on Earth. Since everyday experience tells us that drag heating of cars on the highway or of human skydivers is small (limited to a few Kelvins at most), it must be even smaller (and therefore negligible) for mushballs in Jupiter.

### A3 Parameter sensitivity

We have focused on a set of fiducial model parameters and a simple model to show that mushballs in Jupiter can form and potentially transport ammonia downward efficiently. In Table A1, we study how varying these parameters affect the mushballs characteristics and how far they penetrate into Jupiter’s atmosphere. The pressure at which mushballs evaporate,  $P_{\max}$ , their depth measured from the 1 bar level and the fall duration are provided both for the nominal ventilation factors (Eq. (9) and plain lines in Fig. 3) and for 10 times lower values (dashed lines in Fig. 3).

The first four lines of Table A1 correspond to our fiducial case (Fig. 3), for 4 values of the water ice abundance, from  $\tilde{x}_{\text{H}_2\text{O}} = 100$  to 1200 ppmv. These lead to mushballs similar to the largest hailstones on Earth, with a maximum diameter between about 10 to 18 cm and a maximum mass between 0.1 and 0.9 kg. Their maximum free-fall velocity  $v_{\max}$  can reach more than 200 m/s, reaching full melting pressures  $P_{\max}$  between 6.4 to over 20 bars in as much as 2.7 hours to as little as 30 minutes. The final  $\text{NH}_3$  fraction at evaporation is always high, ensuring an efficient transport of ammonia.

When decreasing the upward velocity  $v_{\text{up}}$  to 10 m/s, the growth of mushballs is suppressed. For all but the highest  $\text{H}_2\text{O}$  values, they melt soon after reaching the  $0^\circ\text{C}$  level at pressures close to 5 – 6 bar. They can reach deeper levels for higher  $\text{H}_2\text{O}$  crystal concentrations, but the value of  $f_{\text{NH}_3}$  is then too low for an efficient transport of ammonia. Conversely, increasing  $v_{\text{up}}$  to 100 m/s leads to a fast mushball growth and a penetration depth that can reach the 27 bar level in the most favorable conditions (including a ventilation factor that is ten times lower than the nominal one).

The value of the range over which a strong updraft is present (nominally between  $P_{\text{bottom}} = 5$  bar and 0.4 bar) has only a limited effect on the outcome, and results with  $P_{\text{bottom}} = 2$  bar are relatively close to the nominal case. Similarly, a change of the initial seed radius of the ice crystal,  $\tilde{d}_0$ , or in the relative humidity above cloud base,  $H_a$ , lead to very small changes in the final results.

Changing  $E_{\text{NH}_3}$ , the collection efficiency in the region where  $\text{NH}_3 \cdot \text{H}_2\text{O}$  forms, leads to a limited suppression of growth for high  $\text{H}_2\text{O}$  ice abundances. However, for  $\tilde{x}_{\text{H}_2\text{O}} = 100$  and 300 ppmv, we notice an increase of the mushball size and penetration instead. This is because for this case, the mushball starts evaporating in a region where the updraft is still present and is transported back upward where it continues to grow. This leads to several cycles of growth and evaporation before the mushball is large enough to fall through the zone and fully evaporate. A full consideration of this case is beyond the scope of this paper, but it is reminiscent of hail on Earth which is known to undergo multiple episodes of growth (Pruppacher & Klett, 1997).

Finally, the last set of cases correspond to an assumed low density of both  $\text{H}_2\text{O}$  and  $\text{NH}_3 \cdot \text{H}_2\text{O}$  ice. They lead to an extremely fast growth of the mushballs in less than 1.5 hours even for the low  $\tilde{x}_{\text{NH}_3}$  case. Of course, these cases are extreme because compaction effects would be expected to be very significant, but they show that the

**Table A1.** Effect of model parameters on mushball characteristics and penetration depth.

$v_{\text{up}}$ [m/s]	$P_{\text{bottom}}$ [bar]	$\tilde{d}_0$ [ $\mu\text{m}$ ]	$H_a$	$\hat{\rho}_{\text{NH}_3}$ [g/cm <sup>3</sup> ]	$\hat{\rho}_{\text{H}_2\text{O}}$ [g/cm <sup>3</sup> ]	$E_{\text{mush}}$	$E_{\text{H}_2\text{O}}$	$E_{\text{NH}_3}$	$\tilde{x}_{\text{H}_2\text{O}}$ [ppmv]	$d_{\text{max}}$ [cm]	$M_{\text{max}}$ [g]	$v_{\text{max}}$ [m/s]	$P_{\text{max}}$ [bar]	depth [km]	Duration [hr]	$f_{\text{NH}_3}$
50.0	5.0	100	1.0	0.3	0.3	1.0	0.3	1.0	100	6.9	63	97	5.5 – 9.7	55.1 – 81.0	2.6 – 2.7	0.50
									300	9.5	166	173	6.5 – 12.4	62.2 – 93.5	1.0 – 1.1	0.40
									600	13.2	399	231	7.1 – 16.1	66.2 – 107.6	0.6 – 0.7	0.25
									1200	18.9	1093	250	8.0 – 21.7	71.3 – 125.6	0.4 – 0.5	0.14
10.0	5.0	100	1.0	0.3	0.3	1.0	0.3	1.0	100	1.5	1	29	5.1 – 6.0	52.3 – 58.4	1.5 – 1.6	0.50
									300	3.2	5	33	5.4 – 7.1	54.7 – 66.3	1.0 – 1.1	0.18
									600	5.4	25	43	5.8 – 8.6	57.4 – 75.0	0.7 – 0.9	0.07
									1200	9.4	132	140	6.4 – 11.6	61.9 – 89.8	0.5 – 0.7	0.02
100.0	5.0	100	1.0	0.3	0.3	1.0	0.3	1.0	100	10.6	221	341	6.4 – 12.1	61.7 – 92.0	2.2 – 2.3	0.50
									300	12.7	468	332	7.2 – 16.0	66.5 – 107.3	1.0 – 1.1	0.40
									600	18.5	1135	317	7.9 – 21.8	70.9 – 125.9	0.7 – 0.8	0.25
									1200	27.5	3427	330	9.0 – 31.0	77.1 – 149.5	0.4 – 0.6	0.14
50.0	2.0	100	1.0	0.3	0.3	1.0	0.3	1.0	100	4.8	24	97	5.8 – 8.1	57.2 – 72.4	1.7 – 1.8	0.50
									300	8.1	116	153	6.4 – 10.8	61.5 – 86.1	0.9 – 1.1	0.40
									600	12.2	325	231	7.0 – 15.1	65.6 – 104.2	0.5 – 0.7	0.25
									1200	17.4	849	250	7.8 – 19.7	70.5 – 119.8	0.3 – 0.5	0.14
50.0	5.0	30	1.0	0.3	0.3	1.0	0.3	1.0	100	6.9	65	97	5.5 – 9.8	55.1 – 81.3	3.1 – 3.2	0.50
									300	9.5	165	173	6.5 – 12.4	62.2 – 93.5	1.2 – 1.3	0.40
									600	13.4	424	245	7.2 – 16.3	66.6 – 108.5	0.7 – 0.8	0.25
									1200	20.1	1321	270	8.1 – 22.9	72.0 – 129.2	0.4 – 0.6	0.14
50.0	5.0	100	0.0	0.3	0.3	1.0	0.3	1.0	100	6.9	63	97	5.7 – 10.1	56.8 – 82.7	2.6 – 2.7	0.50
									300	9.5	166	173	6.6 – 12.7	63.1 – 94.6	1.0 – 1.1	0.40
									600	13.2	399	231	7.2 – 16.5	67.1 – 109.0	0.6 – 0.7	0.25
									1200	18.9	1093	250	8.1 – 22.2	72.2 – 127.1	0.4 – 0.5	0.14
50.0	5.0	100	1.0	0.3	0.3	1.0	0.3	0.3	100	13.1	142	132	6.4 – 10.6	61.6 – 85.3	8.1 – 6.5	0.50
									300	9.7	149	153	6.4 – 12.1	61.2 – 91.9	2.4 – 2.6	0.40
									600	12.4	312	179	6.9 – 14.9	65.2 – 103.4	1.5 – 1.6	0.25
									1200	17.8	895	218	7.7 – 20.3	69.9 – 121.6	0.8 – 1.0	0.14
50.0	5.0	100	1.0	0.1	0.1	1.0	0.3	1.0	100	14.4	180	336	5.9 – 9.2	58.1 – 78.4	1.5 – 1.5	0.50
									300	19.6	611	275	6.7 – 13.3	63.9 – 97.1	0.7 – 0.8	0.40
									600	32.8	2068	241	7.6 – 18.8	69.1 – 116.7	0.5 – 0.6	0.25
									1200	50.5	6914	224	8.7 – 26.7	75.5 – 139.1	0.3 – 0.5	0.14

727 assumed density of ice crystals is an important parameter. In the Earth atmosphere,  
728 graupel particles with mm sizes have densities ranging from 0.05 to 0.9 g cm<sup>-3</sup> (see  
729 Table 2.8 of Pruppacher and Klett (1997)).

730 Overall, Table A1 shows that for a majority of cases, mushballs grow and deliver  
731 below the 5 bar level a mixture with a high concentration of NH<sub>3</sub> ( $f_{\text{NH}_3} > 0.1$ ), in less  
732 than an hour. For all these cases, evaporative downdrafts would be expected to form  
733 and lead to a further transport of ammonia and water in the deep atmosphere. For  
734 highly favorable cases (high updraft velocities, high abundance of H<sub>2</sub>O ice crystals and  
735 high collection rates) mushballs can penetrate deeper than the 20 bar level. However,  
736 although these may look promising to explain the Juno results directly, the evaporation  
737 of water ice takes place at levels below the water cloud where it may not be recycled  
738 efficiently. Instead the events for which water ice evaporate mostly above the water  
739 cloud base and the mushball core is deposited below appear most favorable.

## 740 **Appendix B Nomenclature**

741 Table B1 provides the main quantities used in this article and their default values.

## 742 **Acknowledgments**

743 This paper is dedicated to the memory of our friend and colleague Adam Showman, cu-  
744 rious mind, great scientist and wonderful man. We thank the referees and particularly  
745 Kensuke Nakajima for helpful comments. TG thanks Stéphanie Cazaux, Yohai Kaspi,  
746 Ravit Helled, the IWG and AWG Juno teams for discussions that led to this work  
747 and Gaël Guillot and Flora Bellone for experimental tests on milk downdrafts and on  
748 ice melting in the family oven. T.G. acknowledges support from the *Centre National*  
749 *d'Etudes Spatiales* and the Japan Society for the Promotion of Science. The codes used  
750 to make the figures in this paper are available at <http://doi.org/10.5281/zenodo.3749609>.

**Table B1.** Quantities used in this paper

Quantity	Default value	Description
$x_{\text{NH}_3}$	$360 \times 10^{-6}$	Volume mixing ratio of ammonia in Jupiter's deep atmosphere <sup>a</sup>
$x_{\text{H}_2\text{O}}$	$2600 \times 10^{-6}$	Volume mixing ratio of water in Jupiter's deep atmosphere <sup>b</sup>
$\tilde{x}_{\text{NH}_3}$	–	Volume mixing ratio of condensed ammonia
$\tilde{x}_{\text{H}_2\text{O}}$	–	Volume mixing ratio of condensed water
$r_{\text{NH}_3 \cdot \text{H}_2\text{O}}$	1/2	Ratio of NH <sub>3</sub> to H <sub>2</sub> O molecules in liquid NH <sub>3</sub> · H <sub>2</sub> O
$\tilde{\rho}_{\text{H}_2\text{O}}$	0.3 g/cm <sup>3</sup>	Physical density of water-ice crystals <sup>c</sup>
$\mu_{\text{H}_2\text{O}}$	18 g/mol	Molar mass of H <sub>2</sub> O
$\mu_{\text{NH}_3}$	17 g/mol	Molar mass of NH <sub>3</sub>
$\mu$	2.3 g/mol	Mean molar mass in Jupiter's atmosphere
$E$	0.3 to 1	Collection efficiency of mushballs with ice crystals
$\tilde{d}$	–	Mushball diameter
$g$	2600 cm/s <sup>2</sup>	Jupiter's gravitational acceleration <sup>d</sup>
$v_{\text{fall}}$	–	Terminal velocity
$v_{\text{up}}$	0 to 50 m/s	Updraft velocity
$C_d$	–	Drag coefficient
$N_{\text{Re}}$	–	Reynolds number
$N_{\text{Re,crit}}$	$3 \times 10^5$	Critical Reynolds number above which $C_d = 0.1$
$L_m$	$3.34 \times 10^9$ erg/g	Latent heat of fusion of water ice <sup>e</sup>
$L_v$	$2.52 \times 10^{10}$ erg/g	Latent heat of vaporization of water at 0°C <sup>e</sup>
$P_{\text{sat}}$	–	Saturation pressure of water <sup>f</sup>
$H_a$	0 to 1	Relative humidity above cloud base
$\mathcal{R}$	$8.314463 \times 10^7$ erg/(mol K)	Gas constant
$\tilde{D}_{\text{NH}_3}^{\text{liq}}$	$10^{-5}$ cm <sup>2</sup> /s	Diffusion coefficient of ammonia in liquid water (at ~20°C) <sup>g</sup>
$\tilde{D}_{\text{NH}_3}^{\text{sol}}$	$4 \times 10^{-10}$ cm <sup>2</sup> /s	Diffusion coefficient of ammonia in water ice (at 140 K) <sup>h</sup>
$\tilde{c}_{P,\text{H}_2\text{O}}$	$1.5 \times 10^7$ erg/(g K)	Heat capacity of water ice (at –80°C)
$\tilde{k}_{\text{H}_2\text{O}}$	$3.2 \times 10^5$ erg/(s cm K)	Thermal conductivity of water ice (at –80°C)
————— Quantities varying along a Jupiter atmospheric temperature profile —————		
$P$	[1.0, 17.6] bar	Atmospheric pressure <sup>i</sup>
$T$	[166.1, 400.8] K	Atmospheric temperature <sup>i</sup>
$\rho$	$[1.66, 12.2] \times 10^{-4}$ g/cm <sup>3</sup>	Atmospheric density <sup>i</sup>
$z$	[0, –112.9] km	Altitude from the 1 bar level <sup>i</sup>
$v_{\text{th}}$	[1.10, 1.70] km/s	Thermal velocity
$c_{P,a}$	[3.12, 3.49] $\mathcal{R}$	Heat capacity of normal hydrogen <sup>j</sup>
$\eta_a$	$[5.97, 10.9] \times 10^{-5}$ g/(cm s)	Dynamic viscosity of hydrogen <sup>j</sup>
$\nu_a$	[0.41, 0.10] cm <sup>2</sup> /g	Kinematic viscosity of hydrogen <sup>j</sup>
$K_a$	[0.61, 0.15] cm <sup>2</sup> /s	Thermal diffusivity of hydrogen <sup>j</sup>
$k_a$	$[1.15, 2.35] \times 10^4$ erg/(s cm K)	Thermal conductivity of hydrogen <sup>j</sup>
$D_{\text{NH}_3}$	[0.33, 0.070] cm <sup>2</sup> /s	Diffusion coefficient of ammonia vapor in hydrogen <sup>k</sup>
$D_{\text{H}_2\text{O}}$	[0.39, 0.082] cm <sup>2</sup> /s	Diffusion coefficient of water vapor in hydrogen <sup>k</sup>
$\lambda_{\text{NH}_3}$	[0.09, 0.012] $\mu\text{m}$	Mean free path of ammonia vapor in hydrogen
$\lambda_{\text{H}_2\text{O}}$	[0.11, 0.014] $\mu\text{m}$	Mean free path of water vapor in hydrogen

<sup>a</sup> Li et al. (2017).<sup>b</sup> Assuming a solar N/O ratio (Lodders, 2003).<sup>c</sup> Approximate value based on measurement in Earth clouds (Pruppacher & Klett, 1997).<sup>d</sup> Value obtained using Jupiter's mean radius (Guillot, 2005).<sup>e</sup> [https://en.wikipedia.org/wiki/Latent\\_heat](https://en.wikipedia.org/wiki/Latent_heat).<sup>f</sup> Dean (1999).<sup>g</sup> [https://www.engineeringtoolbox.com/diffusion-coefficients-d\\_1404.html](https://www.engineeringtoolbox.com/diffusion-coefficients-d_1404.html).<sup>h</sup> Livingston et al. (2002).<sup>i</sup> Galileo probe profile (Seiff et al., 1998).<sup>j</sup> NIST Standard Reference Database Number 69, <https://webbook.nist.gov/chemistry/fluid/><sup>k</sup> Cussler (2009)

## References

- 751
- 752 Atreya, S. K., Wong, M. H., Owen, T. C., Mahaffy, P. R., Niemann, H. B., de Pater,  
753 I., ... Encrenaz, T. (1999). A comparison of the atmospheres of Jupiter and  
754 Saturn: deep atmospheric composition, cloud structure, vertical mixing, and  
755 origin. *Planet. Space Sci.*, *47*(10-11), 1243-1262.
- 756 Becker, H., Alexander, J. W., Atreya, S. K., Bolton, S. J., Brennan, M. J., Brown,  
757 S. T., ... Steffes, P. G. (2020). Small lightning flashes from shallow electrical  
758 storms on Jupiter. *Nature*, *in press*.
- 759 Bolton, S. J., Adriani, A., Adumitroaie, V., Allison, M., Anderson, J., Atreya, S.,  
760 ... Wilson, R. (2017). Jupiter's interior and deep atmosphere: The initial  
761 pole-to-pole passes with the Juno spacecraft. *Science*, *356*(6340), 821-825.
- 762 Cussler, E. L. (2009). *Diffusion. Mass Transfer in Fluid Systems*. Cambridge Uni-  
763 versity Press, Cambridge, ed. 3.
- 764 Davidovits, C. R., Kolb, C. E., Williams, L. R., Jayne, J. T., & Worsnop, D. R.  
765 (2006). Mass Accommodation and Chemical Reactions at Gas-Liquid Inter-  
766 faces. *Chem. Rev.*, *106*, 1323-1354.
- 767 de Pater, I., Sault, R. J., Butler, B., DeBoer, D., & Wong, M. H. (2016). Peer-  
768 ing through Jupiter's clouds with radio spectral imaging. *Science*, *352*(6290),  
769 1198-1201.
- 770 de Pater, I., Sault, R. J., Wong, M. H., Fletcher, L. N., DeBoer, D., & Butler, B.  
771 (2019). Jupiter's ammonia distribution derived from VLA maps at 3-37 GHz.  
772 *Icarus*, *322*, 168-191.
- 773 Dean, J. A. (1999). *Lange's Handbook of Chemistry*. McGraw Hill Inc, New York,  
774 ed. 15.
- 775 Gierasch, P. J., Ingersoll, A. P., Banfield, D., Ewald, S. P., Helfenstein, P., Simon-  
776 Miller, A., ... Galileo Imaging Team (2000). Observation of moist convection  
777 in Jupiter's atmosphere. *Nature*, *403*(6770), 628-630.
- 778 Guillot, T. (2005). THE INTERIORS OF GIANT PLANETS: Models and Out-  
779 standing Questions. *Annual Review of Earth and Planetary Sciences*, *33*, 493-  
780 530.
- 781 Guillot, T., Miguel, Y., Militzer, B., Hubbard, W. B., Kaspi, Y., Galanti, E., ...  
782 Bolton, S. J. (2018). A suppression of differential rotation in Jupiter's deep  
783 interior. *Nature*, *555*(7695), 227-230.
- 784 Homann, H., Guillot, T., Bec, J., Ormel, C. W., Ida, S., & Tanga, P. (2016). Effect  
785 of turbulence on collisions of dust particles with planetesimals in protoplan-  
786 etary disks. *A&A*, *589*, A129.
- 787 Hueso, R., Sánchez-Lavega, A., & Guillot, T. (2002). A model for large-scale convec-  
788 tive storms in Jupiter. *Journal of Geophysical Research (Planets)*, *107*(E10),  
789 5075.
- 790 Ingersoll, A. P., Adumitroaie, V., Allison, M. D., Atreya, S., Bellotti, A. A., Bolton,  
791 S. J., ... Steffes, P. G. (2017). Implications of the ammonia distribution on  
792 Jupiter from 1 to 100 bars as measured by the Juno microwave radiometer.  
793 *Geophys. Res. Lett.*, *44*(15), 7676-7685.
- 794 Jin, R., & Chu, L. T. (2007). Uptake of NH<sub>3</sub> and NH<sub>3</sub>+ HOBr Reaction on Ice Sur-  
795 faces at 190 K. *Journal of Physical Chemistry A*, *111*(32), 7833-7840.
- 796 Kargel, J. S. (1992). Ammonia-water volcanism on icy satellites: Phase relations at  
797 1 atmosphere. *Icarus*, *100*(2), 556-574.
- 798 Kargel, J. S., Croft, S. K., Lumine, J. I., & Lewis, J. S. (1991). Rheological prop-  
799 erties of ammonia-water liquids and crystal-liquid slurries: Planetological  
800 applications. *Icarus*, *89*(1), 93-112.
- 801 Kasper, T., Wong, M. H., Marschall, J., de Pater, I., Romani, P. N., & Kalogerakis,  
802 K. S. (2011). Uptake of ammonia gas by Jovian ices. In *Epsc-dps joint meeting*  
803 *2011* (Vol. 2011, p. 352).
- 804 Kessler, E. (1969). On the Distribution and Continuity of Water Substance in Atmo-  
805 spheric Circulation. In M. American Meteorological Society Boston (Ed.), *Me-*

- 806 *teorological monographs, vol 10* (Vol. 10).
- 807 Kundu, P. K., & Cohen, I. M. (2016). *Fluid Mechanics: Sixth Edition*. Academic
- 808 Press, Amsterdam.
- 809 Lewis, J. S. (1969). The clouds of Jupiter and the  $\text{NH}_3$ ,  $\text{H}_2\text{O}$  and  $\text{NH}_3\cdot\text{H}_2\text{S}$  systems.
- 810 *Icarus*, *10*(3), 365-378.
- 811 Li, C., Ingersoll, A., Bolton, S., Levin, S., Janssen, M., Atreya, S., ... Zhang, Z.
- 812 (2020). The water abundance in Jupiter's equatorial zone. *Nature Astronomy*.
- 813 Li, C., Ingersoll, A., Janssen, M., Levin, S., Bolton, S., Adumitroaie, V., ...
- 814 Williamson, R. (2017). The distribution of ammonia on Jupiter from a pre-
- 815 liminary inversion of Juno microwave radiometer data. *Geophys. Res. Lett.*,
- 816 *44*(11), 5317-5325.
- 817 Livingston, F. E., Smith, J. A., & George, S. M. (2002). General Trends for Bulk
- 818 Diffusion in Ice and Surface Diffusion on Ice. *Journal of Physical Chemistry A*,
- 819 *106*(26), 6309-6318.
- 820 Lodders, K. (2003). Solar System Abundances and Condensation Temperatures of
- 821 the Elements. *ApJ*, *591*(2), 1220-1247.
- 822 Nelson, S. P. (1983). The Influence of Storm Flow Structure on Hail Growth. *Jour-*
- 823 *nal of Atmospheric Sciences*, *40*(8), 1965-1983.
- 824 Phillips, V. T. J., Formenton, M., Bansemer, A., Kudzotsa, I., & Lienert, B. (2015).
- 825 A Parameterization of Sticking Efficiency for Collisions of Snow and Graupel
- 826 with Ice Crystals: Theory and Comparison with Observations\*. *Journal of*
- 827 *Atmospheric Sciences*, *72*(12), 4885-4902.
- 828 Pruppacher, H. R., & Klett, J. D. (1997). *Microphysics of Clouds and Precipitation*.
- 829 Kluwer Academic Publishers, Dordrecht, ed. 2.
- 830 Rasmussen, R. M., & Heymsfield, A. J. (1987). Melting and Shedding of Graup-
- 831 pel and Hail. Part I: Model Physics. *Journal of Atmospheric Sciences*, *44*(19),
- 832 2754-2763.
- 833 Rasmussen, R. M., Levizzani, V., & Pruppacher, H. R. (1984). A Wind Tunnel and
- 834 Theoretical Study on the Melting Behavior of Atmospheric Ice Particles: III.
- 835 Experiment and Theory for Spherical Ice Particles of Radius larger than 500
- 836 microns. *Journal of Atmospheric Sciences*, *41*(3), 381-388.
- 837 Rogers, R. R., & Yau, M. K. (1996). *A short course in cloud physics*. Elsevier.
- 838 Roos, D. V. D. S. (1972). A Giant Hailstone from Kansas in Free Fall. *Journal of*
- 839 *Applied Meteorology*, *11*(6), 1008-1011.
- 840 Seiff, A., Kirk, D. B., Knight, T. C. D., Young, R. E., Mihalov, J. D., Young, L. A.,
- 841 ... Atkinson, D. (1998). Thermal structure of Jupiter's atmosphere near
- 842 the edge of a 5- $\mu\text{m}$  hot spot in the north equatorial belt. *J. Geophys. Res.*,
- 843 *103*(E10), 22857-22890.
- 844 Showman, A. P., & de Pater, I. (2005). Dynamical implications of Jupiter's tropo-
- 845 spheric ammonia abundance. *Icarus*, *174*(1), 192-204.
- 846 Stein, R. F., & Nordlund, Å. (1998). Simulations of Solar Granulation. I. General
- 847 Properties. *ApJ*, *499*(2), 914-933.
- 848 Stoker, C. R. (1986). Moist convection: A mechanism for producing the vertical
- 849 structure of the Jovian Equatorial Plumes. *Icarus*, *67*(1), 106-125.
- 850 Sugiyama, K., Nakajima, K., Odaka, M., Kuramoto, K., & Hayashi, Y. Y. (2014).
- 851 Numerical simulations of Jupiter's moist convection layer: Structure and dy-
- 852 namics in statistically steady states. *Icarus*, *229*, 71-91.
- 853 Turner, J. S. (1969). Buoyant Plumes and Thermals. *Annual Review of Fluid Me-*
- 854 *chanics*, *1*(1), 29-44.
- 855 Weidenschilling, S. J., & Lewis, J. S. (1973). Atmospheric and cloud structures of
- 856 the Jovian planets. *Icarus*, *20*(4), 465-476.
- 857 Yair, Y., Levin, Z., & Tzivion, S. (1995). Microphysical processes and dynamics of a
- 858 Jovian thundercloud. *Icarus*, *114*(2), 278-299.



Figure 1.

Author Manuscript

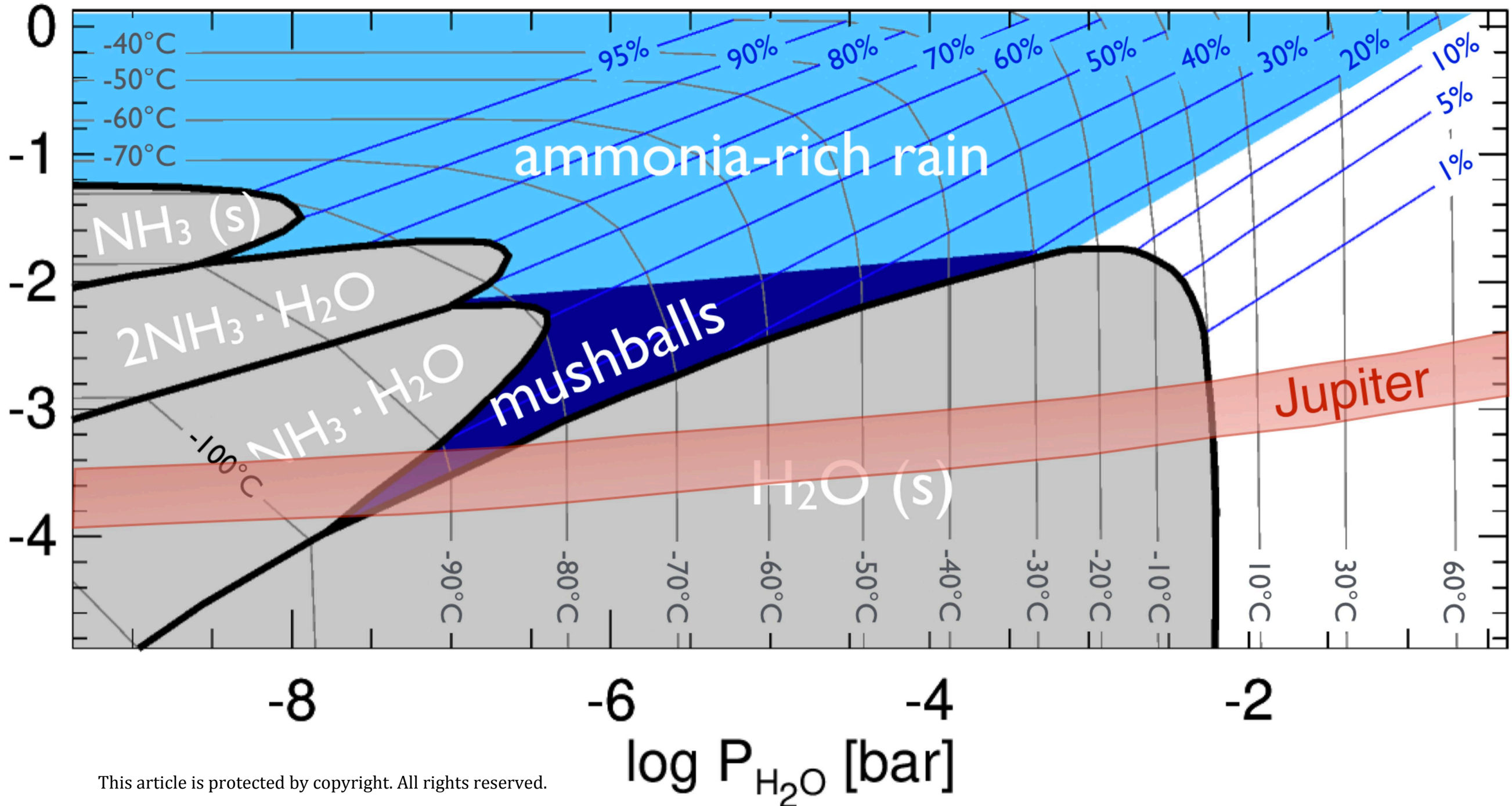


Figure 2.

Author Manuscript

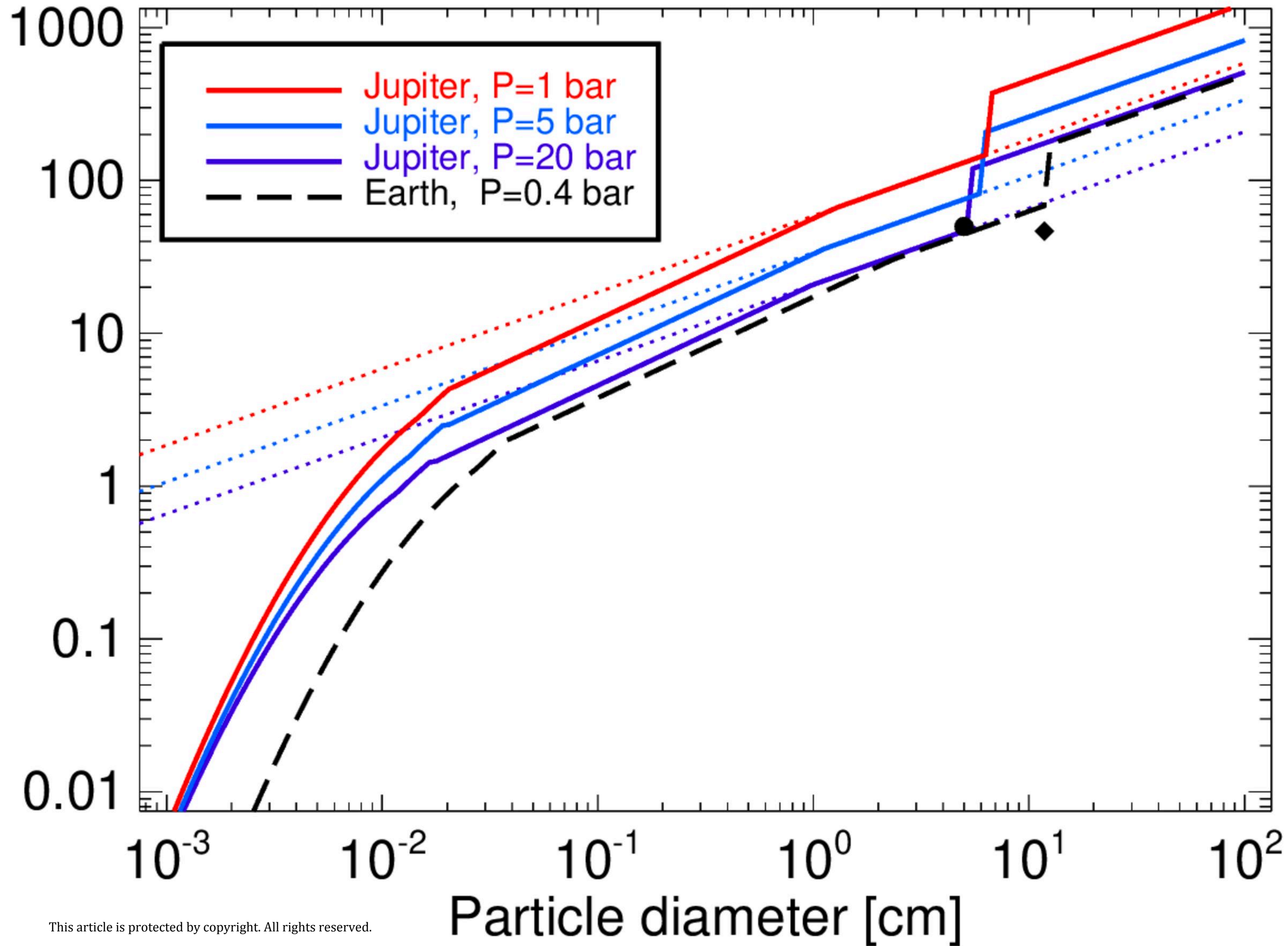


Figure 3.

Author Manuscript



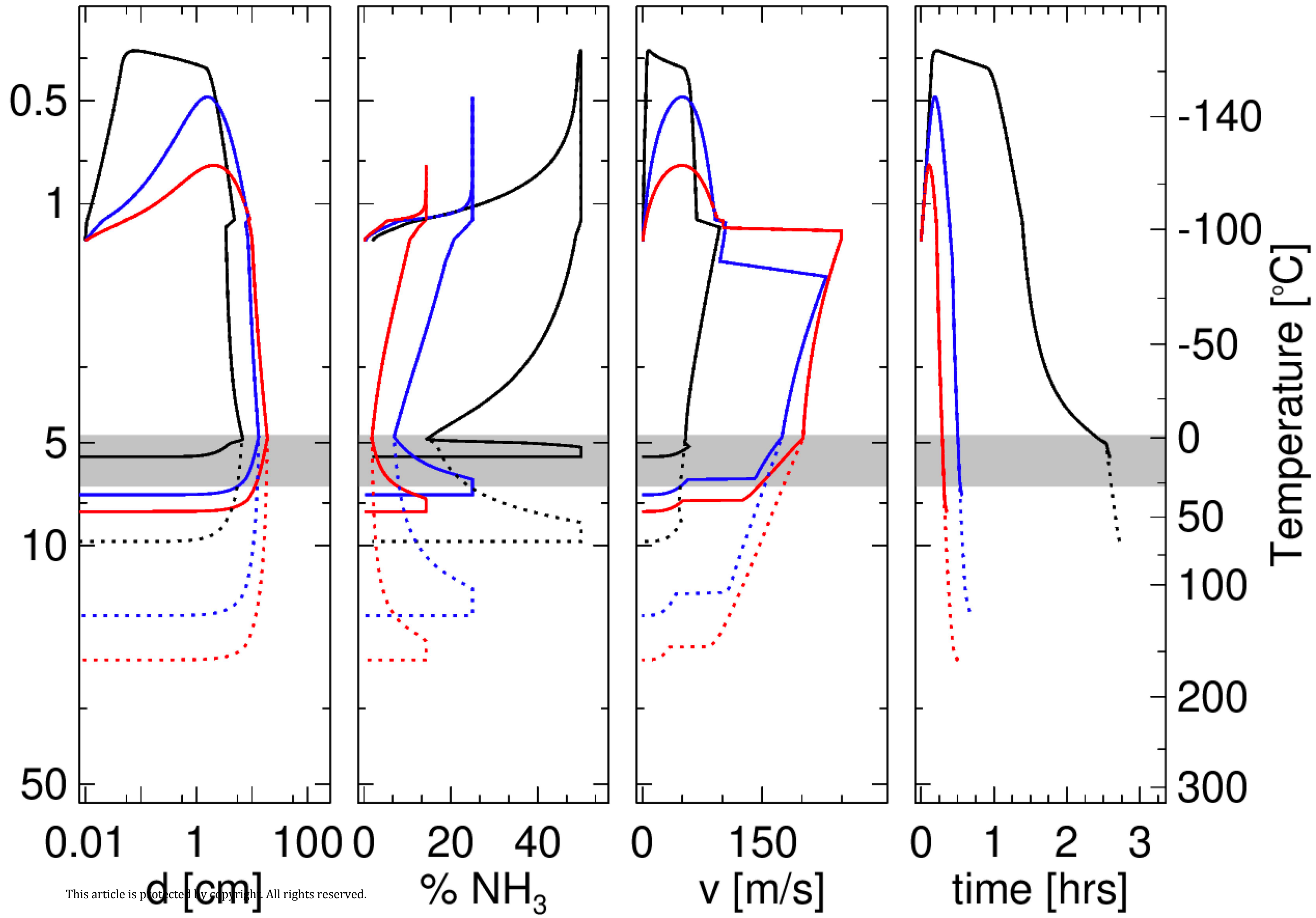




Figure 4.

Author Manuscript



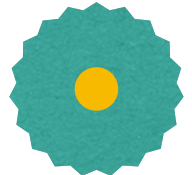

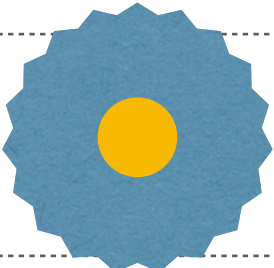


Phase	Morphology	Size	Pressure	Comments
0		10-100 $\mu$ m	4.5-1.1 bar	H <sub>2</sub> O ice crystal
1		100 $\mu$ m-1mm	1.5-1.1 bar	H <sub>2</sub> O · NH <sub>3</sub> liquid + H <sub>2</sub> O ice slush
2		1mm-5cm	1.1-0.5 bar	H <sub>2</sub> O · NH <sub>3</sub> liquid core surrounded by shell of low density H <sub>2</sub> O · NH <sub>3</sub> ice and H <sub>2</sub> O ice
3		2-3cm	1.1-1.5 bar	H <sub>2</sub> O · NH <sub>3</sub> liquid core surrounded by H <sub>2</sub> O ice shell
4		3-10cm	1.5-5 bar	H <sub>2</sub> O · NH <sub>3</sub> liquid core surrounded by H <sub>2</sub> O ice shell (possibly porous away from the core)
5		10-2cm	5-10 bar	H <sub>2</sub> O · NH <sub>3</sub> liquid core H <sub>2</sub> O ice crust H <sub>2</sub> O water shell
6		2-0cm	7-11 bar	Evaporating H <sub>2</sub> O · NH <sub>3</sub> liquid droplet

Figure 5.

Author Manuscript









